Heat and drought events alter biogenic capacity to balance CO_2 budget in south-western Europe

R. Segura-Barrero[1], T. Lauvaux[2], J. Lian[3,4], P. Ciais[4], A. Badia[1], S. Ventura[1], H. Bazzi[5,6], E. Abbessi[4], Z. Fu[4] and G. Villalba[1,7]

[1]Sostenipra Research Group, Institute of Environmental Sciences and Technology, Z Building, Universitat Autònoma de Barcelona (UAB), Campus UAB, 08193 Bellaterra, Barcelona, Spain.

[2]Molecular and Atmospheric Spectrometry Group (GSMA) – UMR 7331, University of Reims Champagne Ardenne, France.

[3]Origins earth, Suez Group, Tour CB21, 16 Place de l'Iris, 92040 La Défense, Paris CEDEX, France.

[4]Laboratoire des Sciences du Climat et de l'Environnement (LSCE), IPSL, CEA-CNRS-UVSQ, Université Paris-Saclay, 91191 Gif-sur-Yvette CEDEX, France.

[5]Université Paris-Saclay, AgroParisTech, INRAE, UMR 518 MIA Paris-Saclay, 91120 Palaiseau, France.

[6]Atos France, Technical Services, 80 Quai Voltaire, 95870 Bezons, France.

[7]Department of Chemical, Biological and Environmental Engineering, Universitat Autònoma de Barcelona (UAB), Campus UAB, 08193 Bellaterra, Barcelona, Spain.

Corresponding author: Gara Villalba (gara.villalba@uab.cat)

Key Points:

- We modify the Vegetation Photosynthesis and Respiration Model to include soil moisture impacts on ecosystem carbon fluxes.
- A modest annual increase of net cabon sink of 0.80 gC/m^2year is found in south-western Europe but with high spatial and annual variability.
- The interannual net ecosystem exchange variability is more influenced by drought in temperate humid regions than in Mediterranean semi-arid regions.
- The heatwave and drought event of 2022, reduced net ecosystem exchange by 78.5 TgC, a 27% decrease from the mean.

Abstract

Heat and drought events are increasing in frequency and intensity, posing significant risks to natural and agricultural areas with uncertain effects on the net ecosystem CO_2 exchange (NEE). We modified the Vegetation Photosynthesis and Respiration Model to include soil moisture impacts on the gross ecosystem exchange (GEE) and respiration (R_{ECO}) fluxes and determine the temporal variability of NEE over south-western Europe for 2001-2022. Warming temperatures lengthen growing seasons causing an increase in GEE which is mostly compensated by a similar increment in R_{ECO}, resulting in a modest annual increase of net carbon sink of 0.80 gC/m^2year but with high spatial and annual variability. The heatwave of 2022 reduced NEE by 78.5 TgC, a 27% decrease from the mean. The interannual variability is more influenced by drought in temperate humid regions than in Mediterranean semi-arid regions. These results emphasize the vulnerability of the net carbon sink as drying trends could revert the NEE trends, as it is happening for croplands in the French Central Massif.

1 Introduction

Global Global climate change and the increasing occurrence of extreme climate events are profoundly impacting the terrestrial carbon balance, altering vegetation dynamics, and influencing the net carbon uptake from ecosystems (Ciais et al., 2005; Keenan et al., 2016; Reichstein et al., 2013). Climate warming has extended the growing season in Northern ecosystems by producing more favorable conditions for photosynthesis, thereby increasing their terrestrial ecosystem productivity or gross ecosystem exchange (GEE) (Ciais et al., 2019; Zhu et al., 2016). The increased atmospheric carbon dioxide (CO_2) concentrations also have positive fertilization effects on the vegetation productivity (Los, 2013; Schimel et al., 2015; Thornton et al., 2007). However, warming has also stimulated the release of terrestrial carbon to the atmosphere or ecosystem respiration (R_{ECO}), by enhanced soil organic matter decomposition and vegetation respiration (Keenan et al., 2016). Interannual variations of biogenic carbon fluxes are expected to increase with increasing frequency and intensity of extreme climate events (Zscheischler, Mahecha, et al., 2014; Zscheischler, Reichstein, et al., 2014), potentially destabilizing the long-term carbon cycle (Fernández-Martínez et al., 2023). These trends depend on vegetation and local climate. For example, arid and semi-arid regions, such as the southern Iberian Peninsula and northern Africa, present higher interannual variations of GEE (Zhang et

al., 2016). On the other hand, GEE in humid benefit from the CO_2 fertilization and the longer growing seasons in high latitudes responsible for larger GEE trends compared to other regions (Zhang et al., 2016).

There is an urgent need to better understand how warming and drying trends affect the vegetation in transition regions like south-western Europe. Recent studies have focused on southern Europe, one of the key regions impacted by climate change (Giorgi & Lionello, 2008), with an increasing frequency and intensity of heat and drought events (Fischer & Schär, 2010; Molina et al., 2020). Over the last two decades, observable impacts have been observed (Barriopedro et al., 2011; Vicente-Serrano et al., 2014), which pose significant risks to crops and natural ecosystems. Although the Mediterranean climate is typically characterized by long dry summers (Gilabert et al., 2015), the resilience of its forests (Gazol et al., 2018) reaches its limits when long drought episodes combined with heat waves start to affect the vegetation, leading to a reduction of the net atmospheric CO_2 capture by the ecosystems or net ecosystem exchange (NEE). It is crucial to comprehend the impact of heat and drought events on the south-western European carbon balance.

In recent years, the south-western European region has faced a series of droughts and hot episodes. In France and Central Europe, air temperatures during the summer 2003 were the highest in the last 500 years, which caused a reduction of the continental net carbon uptake in the range of 20 – 500 TgC $year^{-1}$, and in some regions changing the ecosystems from carbon sinks to carbon sources (Ciais et al., 2005; Reichstein et al., 2007). The Iberian Peninsula experienced droughts in 2004/2005, 2012, 2015, 2017 and 2022, which produced detrimental effects on the ecosystems, and combined with high summer temperatures intensified the occurrence of fires in the territory (Ermitão et al., 2021; Faranda et al., 2023; Ionita et al., 2017; Nunes et al., 2019; Sánchez-Benítez et al., 2018). In Italy, the summers of 2003, 2017 and 2022 with exceptional temperatures which combined with persistent soil water deficits, resulted into extreme impacts on vegetation productivity (Faranda et al., 2023; Rita et al., 2020; Trucchia et al., 2022). The exceptional drought of the summer 2022, affecting central and south-eastern Europe, caused a reduction of the net biosphere uptake in summer between 56 and 62 TgC over the drought area (van der Woude et al., 2023). While different studies have investigated the role of water and heat stress on GEE in southern Europe (Ermitão et al., 2021; Gilabert et al., 2015; Gouveia et al., 2017; Rita et al., 2020), changes in the net ecosystem exchange remains highly uncertain due to

complex dependencies from heat and drought episodes on ecosystem respiration R_{ECO} (Reichstein et al., 2013; von Buttlar et al., 2018).

While the impact of heat and drought events on the carbon balance has been well studied for central and northern Europe (Bastos et al., 2020; Ciais et al., 2005; Ramonet et al., 2020), a multi-year analysis for south-western Europe is lacking. South-western Europe has less long-term observational records of CO_2 concentrations and fluxes, which constrains the understanding of regional biogenic carbon dynamics. Additionally, soil water availability and vapor pressure deficit (atmospheric dryness) are the main factors driving interannual variability of photosynthesis (Gilabert et al., 2015), but the timing of drought and heat events are also important factors in the vegetation response (Jin et al., 2023). Moreover, process-based biogeochemical models usually fail at capturing the vegetation carbon response to extreme variations in soil moisture (Stocker et al., 2018, 2019).

Remote sensing data-driven biosphere models, which estimate ecosystem fluxes based on satellite vegetation indices and meteorological drivers, usually estimate the water stress effect on GEE using satellite sensed water indices or the vapor pressure deficit without considering soil moisture as a model input (Fu et al., 2022; Stocker et al., 2018, 2019). Although satellite indices can capture to some extent the effect of droughts on GEE (Maselli et al., 2009), they tend to underestimate the magnitude of GEE reductions under dry conditions (Stocker et al., 2019). For instance, the Vegetation Photosynthesis and Respiration Model (VPRM) (Mahadevan et al., 2008) does not consider soil moisture as a driver (Mahadevan et al., 2008). Different studies have shown the potential of enhancing the VPRM model capabilities by model parameters optimization (Dayalu et al., 2018) or by modifying the respiration equation (Gourdji et al., 2022), resulting in similar or even better model performances compared to more complex process-based models.

The main objective of this study is to determine the effect of heat and drought events on the temporal variability of the net biogenic carbon fluxes over south-western Europe, including Portugal, Spain, southern France, and Italy. To do so, we modify the VPRM model to represent the impact of soil moisture on the GEE and R_{ECO} for the period 2001-2022. In addition to the analysis of long-term carbon fluxes variability over this whole period we also study the control of climate driver anomalies (temperature, soil moisture and solar radiation) and drought indices

as the Standardized Precipitation Evaporation Index (SPEI) (Vicente-Serrano et al., 2010, 2013) on the carbon fluxes interannual anomalies over ten biogeographical regions (Figure 1). To complement the analysis of VPRM simulations, we also estimate GEE based on the sun-induced chlorophyll fluorescence (SIF) provided by the Global Orbiting Carbon Observatory-2 (OCO-2) SIF product (GOSIF) (Li & Xiao, 2019). Finally, we also study the intra-annual variations in carbon fluxes during three exceptional heat and drought events: Western Europe region in the year 2003, the Iberian sclerophyllous region in the year 2005, and the Atlantic region in the year 2022.

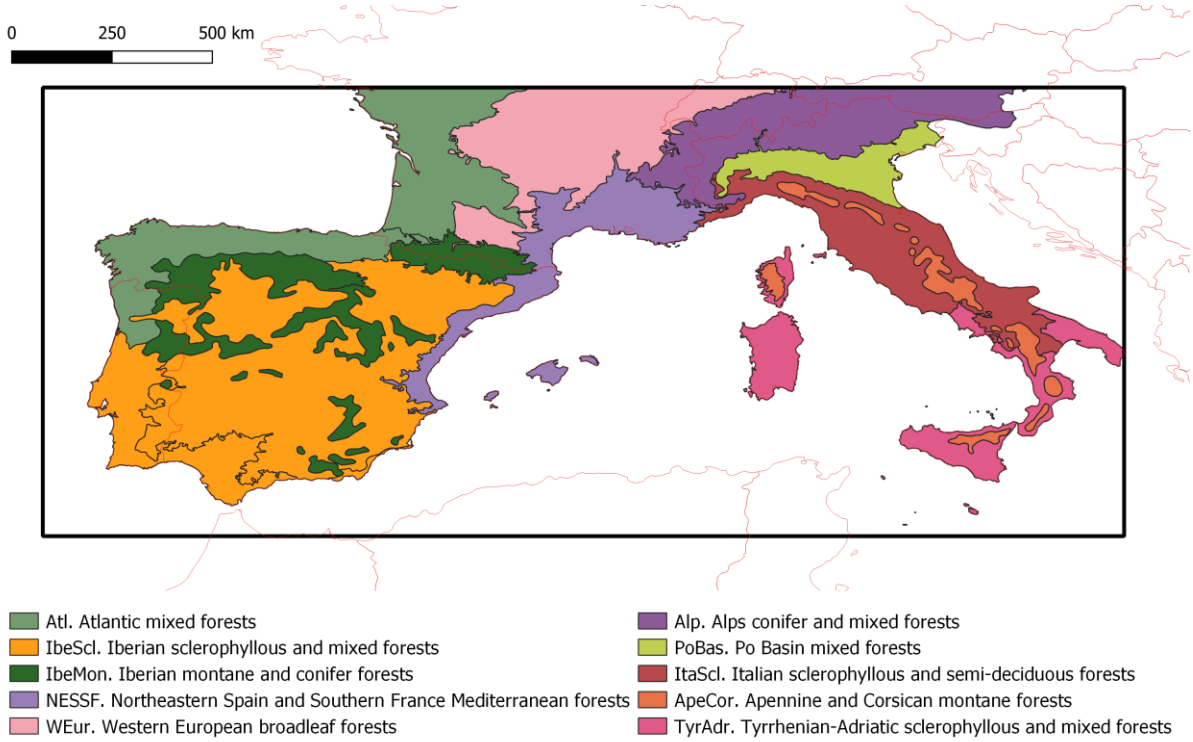

Figure 1. Area of study and biogeographical regions of this study.

2 Materials and Methods

2.1 Study area

The study region encompasses south-western Europe from Portugal to Italy (Figure 1). This large area presents a great diversity of ecosystems, topographical features, climates, land-uses, and soil

typologies (Gouveia et al., 2017), which we classify into 10 biogeographical regions based on the map of Terrestrial Ecoregions of the World from the World Wildlife Fund (Olson et al., 2001). The prevailing climate is the subtropical Mediterranean climate, with hot and dry summers, although other climates are present such as temperate oceanic (Atlantic part of France, north of Portugal and Spain), mountainous (high-altitude regions of the Alps, Pyrenees, and Dinaric Alps) and humid continental (Central Europe and north-eastern Italy) climates.

2.2 VPRM modifications

VPRM simulates surface CO_2 exchanges between the atmosphere and the biosphere using meteorological data and remote-sensing vegetation indices (cf. Supporting information). NEE is estimated as the difference between R_{ECO} and GEE, following a negative sign convention where negative fluxes represent CO_2 uptake by ecosystems. VPRM parameters are optimized for 8 plant functional types (PFT) representing various land cover types (i.e. evergreen, deciduous, mixed forest, shrubland, Mediterranean savanna, cropland, grassland, and sparsely vegetated), weighted by fractional coverage to calculate the regional ecosystem fluxes.

To account for the impact of soil moisture on GEE and R_{ECO}, modifications were made in the VPRM equations, with an R_{ECO} parameterization based on (Migliavacca et al., 2011). The methodology for optimizing the modified VPRM parameters and the evaluation using data from southern Europe flux tower observations is presented in the Supporting information.

The GEE parameterization consists of a light-use-efficiency approach that relates the GEE to the fraction of photosynthetically active radiation that is absorbed by the vegetation, combined with a set of optimized scaling factors (λ_{SW}, T_{scale}, W_{scale} and P_{scale}). We introduce a new scaling factor, SM_{scale}, to better represent soil moisture stress on GEE, distinguishing between energy-limited (adequate soil water) and water-limited regimes (insufficient soil water), according to (Stocker et al., 2019). The GEE parameterization is defined as:

$$GEE = \lambda_{SW} \cdot T_{scale} \cdot W_{scale} \cdot P_{scale} \cdot SM_{scale} \cdot \frac{SW}{(1+SW/SW_0)} \cdot EVI \quad (1)$$

with SW, shortwave radiation, SW_0, the half-saturation shortwave radiation, and EVI, the enhanced vegetation index. The function SM_{scale} is defined to be 1 when the soil moisture (θ) is

above a critical soil moisture threshold (θ^*) and decreases linearly below this threshold (Fu et al., 2022). Soil moisture in the uppermost soil level (0-15 cm depth), is normalized between the permanent wilting point and the field capacity of the soil. The form of the SM_{scale} function is:

$$SM_{scale} = \begin{cases} q \cdot (\theta - \theta^*) + 1, & \theta < \theta^* \\ 1, & \theta \geq \theta^* \end{cases} \quad (2)$$

where q and θ^* are optimized parameters. With this modification, we increase the number of parameters in the GEE parameterization from two (λ_{SW}, SW_0) to four (adding q and θ^*).

The default VPRM employs a linear function of air temperature to determine R_{ECO}. In this study, we use an equation proposed in (Reichstein et al., 2003) and (Migliavacca et al., 2011). In our approach, we employ soil moisture, represented by a hyperbolic tangent function, to depict water stress on R_{ECO}, rather than precipitation. This choice is due to soil moisture's superior role in influencing both autotrophic and heterotrophic respirations, driving soil microbial processes and plant stress (W. Liu et al., 2009). The R_{ECO} equation in the modified VPRM relies on air temperature, soil moisture and short-term vegetation productivity (daily GEE) as follows:

$$R_{ECO} = (R_0 + k_1 \cdot GEE) \cdot tanh(k_2 \cdot \theta + \gamma) \cdot e^{E_0 \cdot \left(\frac{1}{T_{ref} - T_0} - \frac{1}{T - T_0}\right)} \quad (3)$$

GEE represents the average GEE over the previous 24 hours, and T is the air temperature. T_{ref} and T_0 are fixed temperatures at 288.15 K (15 °C) and 227.13 K (-46.02 °C), respectively. Model-specific constants, R_0, k_1, k_2, γ and E_0 vary for each PFT and refer to reference abiotic ecosystem respiration, sensitivity of ecosystem respiration to GEE, sensitivity of the ecosystem to soil moisture, a constant indicating how R_{ECO} responds to null θ, and the activation energy parameter for the sensitivity of R_{ECO} to air temperature, respectively. Including vegetation productivity in the respiration parameterization enhances the spatial and temporal dynamics of R_{ECO}, preventing a bias in seasonal amplitude (Migliavacca et al., 2011). Air temperature influences R_{ECO} with non-linear dependencies (Jolly et al., 2005; Reichstein et al., 2003), which can be represented using an Arrhenius type equation, as employed in this parameterization.

The VPRM model is used to estimate biogenic carbon fluxes (NEE, GEE and R_{ECO}) at an hourly resolution spanning from 2001 to 2022 at a spatial resolution of 9 km. The model uses meteorological drivers from the ERA5-Land dataset (Muñoz-Sabater, 2019) and satellite vegetation indices processed from MODIS surface reflectances (Vermote, 2015). The model computes fluxes individually for each PFT and results were subsequently aggregated based on VPRM PFT map. Another modification to VPRM includes differentiating between summer and winter crops within the cropland PFT, as it is explained in the Supporting information.

2.3 Climate and remotely sensed data

Climatic driver data for the VPRM model are from the European Centre for Medium-Range Weather Forecasts (ECMWF) ERA5-Land reanalysis product. These data cover the years 2001 to 2022, with hourly frequency and 0.1o resolution (Muñoz-Sabater, 2019). The key variables used include 2m temperature (T2M) for air temperature, surface solar radiation downwards (SSRD) for shortwave radiation, and volumetric soil water of the second layer (7 to 28 cm depth; SM2) for soil moisture. This specific soil layer is chosen due to its higher correlation with observed soil water content from flux tower stations, compared to other layers.

To assess drought episodes across south-western Europe, monthly averaged ERA5-Land variables, including T2M, SSRD and SM2, are employed. Monthly anomalies for these variables are calculated as the difference with monthly mean between 2001 and 2022. Additionally, the Standardized Precipitation Evaporation Index (SPEI) is computed at various months

aggregations to assess drought intensity and variability using monthly averaged ERA5-Land data. The SPEI aggregated over 1-, 3-, 6-, 9- and 12-months are named respectively SPEI01, SPEI03, SPEI06, SPEI09 and SPEI12. SPEI is a multi-scalar drought index that considers not only precipitation but also the hydrological balance with atmospheric evaporative demand crucial for studying vegetation impacts in warm regions (Vicente-Serrano et al., 2010, 2013). The computation of SPEI is explained in the Supporting information.

The EVI and the land surface water index (LSWI), are processed from the MODIS Terra satellite MOD09A1 v006 product (Vermote, 2015) using the VPRM preprocessor from the Department of Biogeochemical Systems in the Max Planck Institute for Biogeochemistry (https://www.bgc-jena.mpg.de/bgc-systems/pmwiki2/pmwiki.php/Download/VPRMpreproc).

The VPRM model uses the Synergetic Land Cover Product (SYNMAP) (Jung et al., 2006) for the vegetation classification map. SYNMAP is a 1-km global land cover product built from remote sensing observations and its classes are defined based on PFT mixtures with explicit leaf type and longevity definitions, ideal for carbon cycle modelling applications. The 48 land classes of the SYNMAP map were reclassified in the VPRM preprocessor to the 8 VPRM PFT.

To complement the analysis of VPRM simulations, we also estimate GEE based on the sun-induced chlorophyll fluorescence (SIF) provided by the Global Orbiting Carbon Observatory-2 (OCO-2) SIF product (GOSIF), following the methodology outlined by Li and Xiao (2019). GOSIF exhibits strong correlations with GEE at hourly, monthly, and annual scales, maintaining a high correlation with GEE even during drought episodes (Lv et al., 2023; Qiu et al., 2022), and offers the advantage of relying solely on satellite SIF observations, eliminating the need for climate data.

2.4 Statistical analysis

Monthly anomalies of GEE, R_{ECO}, and NEE are calculated at 9 km resolution, as the difference to monthly means (g C m^{-2} $month^{-1}$) for the entire period 2001-2022. The methodology used to determine the long-term trend of the fluxes is detailed in Supporting information. This consists of a linear regression of the carbon fluxes anomalies time series and the significance of these trends is assessed using a Pearson correlation test.

To investigate the influence of SPEI at various timescales on the interannual variability of fluxes, a Pearson correlation analysis is conducted using the time series of detrended flux anomalies. In the case of the climate drivers (T2M, SM2 and SSRD), the partial correlation coefficient is calculated for each variable controlling the interannual variations in the other two driver variables. For this analysis, detrended anomalies are aggregated annually and for growing season months, identified for each biogeographical region and average seasonal cycles. Growing season months are determined based on when GOSIF GEE exceeds 30% of the intra-annual GEE range. Although GOSIF GEE and VPRM GEE generally exhibit similar seasonal cycles across all biogeographical regions, discrepancies are observed for the Iberian and Tyrrhenian-Adriatic sclerophyllous regions (Figure S1).

Finally, we select three study cases consisting of years with severe heat and drought events affecting largely the NEE of the south-western European ecosystems, to study intra-annual variations in biogenic carbon fluxes in response to these major events. The study cases are the Western Europe region in the year 2003, the Iberian sclerophyllous region in the year 2005, and the Atlantic region in the year 2022. For these three study cases, VPRM-simulated biogenic fluxes are aggregated on an 8-daily basis, along with T2M and SM2. Anomalies relative to the means over the 2001-2022 period are computed for each grid cell and 8-daily period within the year.

3 Results

3.1 Trends of south-western Europe biogenic carbon fluxes

The long-term analysis of biogenic carbon fluxes from both VPRM and GOSIF shows an overall increase of both GEE and R_{ECO}, with certain regions of flux stability (Figure 2). GOSIF presents a positive trend in GEE (spatial median of 5.51 g C m^{-2} $year^{-2}$ and 53.4% of the vegetated areas in the domain have a significant increase in GEE), while VPRM positive GEE trends are limited to the mountainous regions. Both models are consistent in estimating a non-significant negative trend in the GEE in the Massif Central mountains (south-central France) and the south-west of the Iberian Peninsula. Both models agree that the Apennine and Corsican biogeographical region presents the highest positive trends (spatial medians of 8.97 and 10.25 g

C m^{-2} $year^{-2}$ for GOSIF and VPRM, respectively), and Western Europe the lowest trends (2.75 and 1.25 g C m^{-2} $year^{-2}$) (see Figure S2 in the Supporting information).

The long-term trends of the VPRM R_{ECO} present a similar spatial distribution to the trends of GEE, although the magnitude is smaller (spatial median of 3.06 g C m^{-2} $year^{-2}$) than for the GEE (3.75 g C m^{-2} $year^{-2}$). Based on the VPRM, the spatial extent of the areas with significant R_{ECO} trends (37.6%) extends further than the areas with significant GEE trends (27.2%), reflecting that the ecosystem respiration has a steadier increase than the gross ecosystem exchange.

This similar spatial distributions of the trends of the GEE and R_{ECO} reflect that long-term variations in released and captured carbon by the ecosystems compensate each other, implying in a trend approaching zero in the NEE (-0.80 g C m^{-2} $year^{-2}$) (Figure 2d). VPRM estimates a significant annual increase of net carbon sink over specific regions located in the Alps (-2.35 g C m^{-2} $year^{-2}$), and the Apennines, and Corsican (-3.83 g C m^{-2} $year^{-2}$) mountainous regions (Figure S2). Only one region shows a decrease in net carbon sink (maximum trends of 11.69 g C m^{-2} $year^{-2}$) over the 2001-2022 period, located in the northern part of the Massif Central, although not statistically significant.

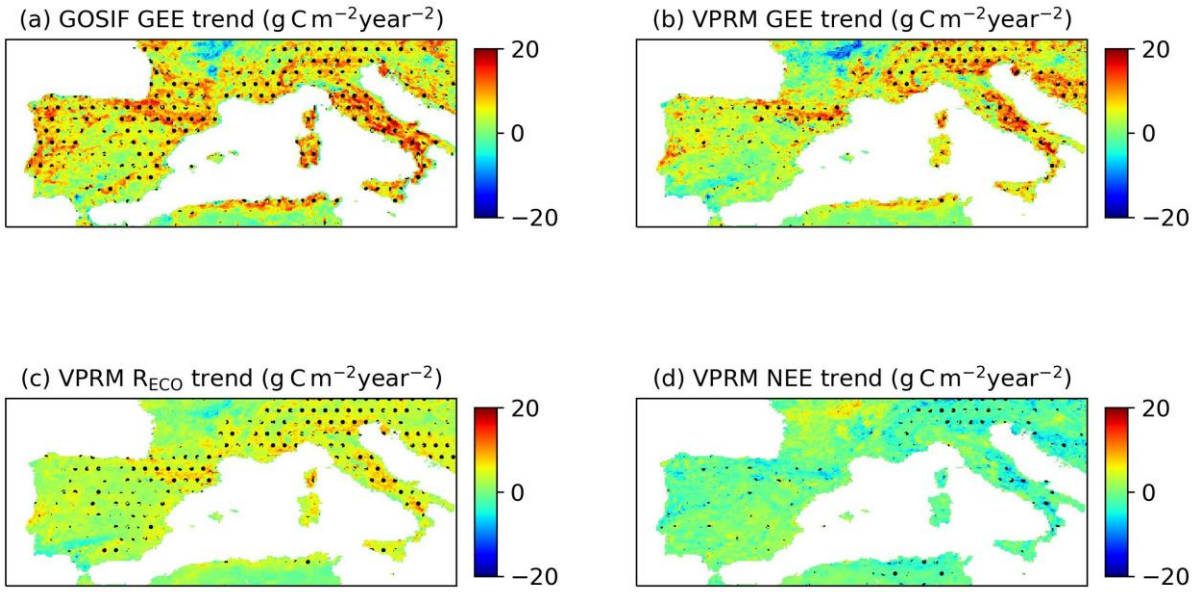

Figure 2. Long-term carbon flux trends. Spatial pattern of the long-term trends of annual fluxes for (a) GOSIF GEE; (b) VPRM GEE; (c) VPRM R_{ECO}; (d) VPRM NEE between 2001 and 2022. The black dots correspond to areas where the linear regression is significant ($p < 0.05$).

The seasonal analysis of the biogenic carbon flux trends show that spring is the season when GEE and R_{ECO} (NEE) exhibited higher (lower) values (Figure S3). During spring, the spatial medians of annual trends are of 0.66, 0.54, 0.31 and -0.24 g C m^{-2} $month^{-1}$ $year^{-1}$ for the GOSIF GEE, VPRM GEE, R_{ECO}, and NEE, respectively. Larger discrepancies between GOSIF and VPRM GEE are present during summer, with 0.43 and 0.08 g C m^{-2} $month^{-1}$ $year^{-1}$, respectively (Figure S3).

The disaggregation of the fluxes by plant functional types (PFT) reveals that the increase in the long-term trends of the GEE and R_{ECO} in the Po Basin, the Italian sclerophyllous, the Apennine and Corsican montane and the Tyrrhenian-Adratic sclerophyllous regions is mainly located over croplands (Figure 3). In other regions such as the Atlantic, the Iberian sclerophyllous and the Western European broadleaf regions, the long-term trends of the respiration are higher than for the GEE in croplands, counteracting the contributions of the natural PFT with stronger sink increases.

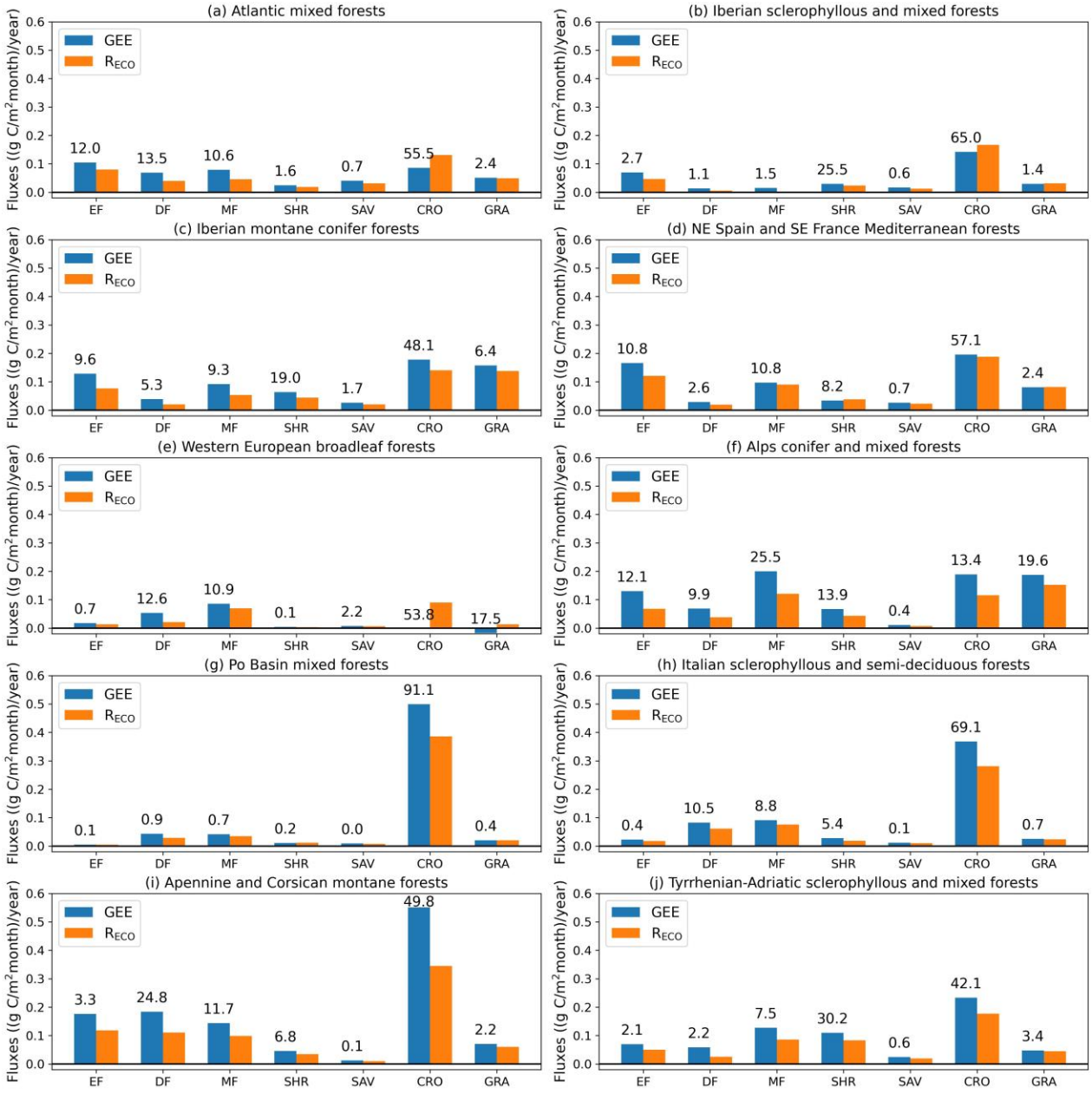

Figure 3. Long-term carbon flux trends by PFT. Average annual trends of the GEE and R_{ECO} aggregated annually for the different biogeographical regions and integrated for the different plant functional types. The PFT percent coverage in each biogeographical region is marked over each bar. EF: evergreen forest, DF: deciduous forest, MF: mixed forest, SHR: shrubland, SAV: savanna, CRO: cropland, GRA: grassland.

Over the entire study area (Figure 4), both VPRM and GOSIF present a significant increase of the annual GEE of 6.5 and 9.4 Tg C $year^{-2}$, respectively. Both GOSIF and VPRM

show a strong agreement on the interannual variability of the GEE. VPRM also presents a significant increase in R_{ECO} of 5.0 Tg C $year^{-2}$. This occurs in conjunction with a significant warming trend of 0.057 °C $year^{-1}$ and a non-significant soil drying trend of -0.0003 m^3m^{-3} $year^{-1}$ over the region. Due to the compensation between GEE and R_{ECO}, the VPRM model shows a non-significant decrease in NEE in the study area of -1.5 Tg C $year^{-2}$. Moreover, the occurrence of summer heat and drought events increases the intra-annual variability of NEE, producing the largest positive NEE anomalies and contributing to destabilize the negative trend in the NEE.

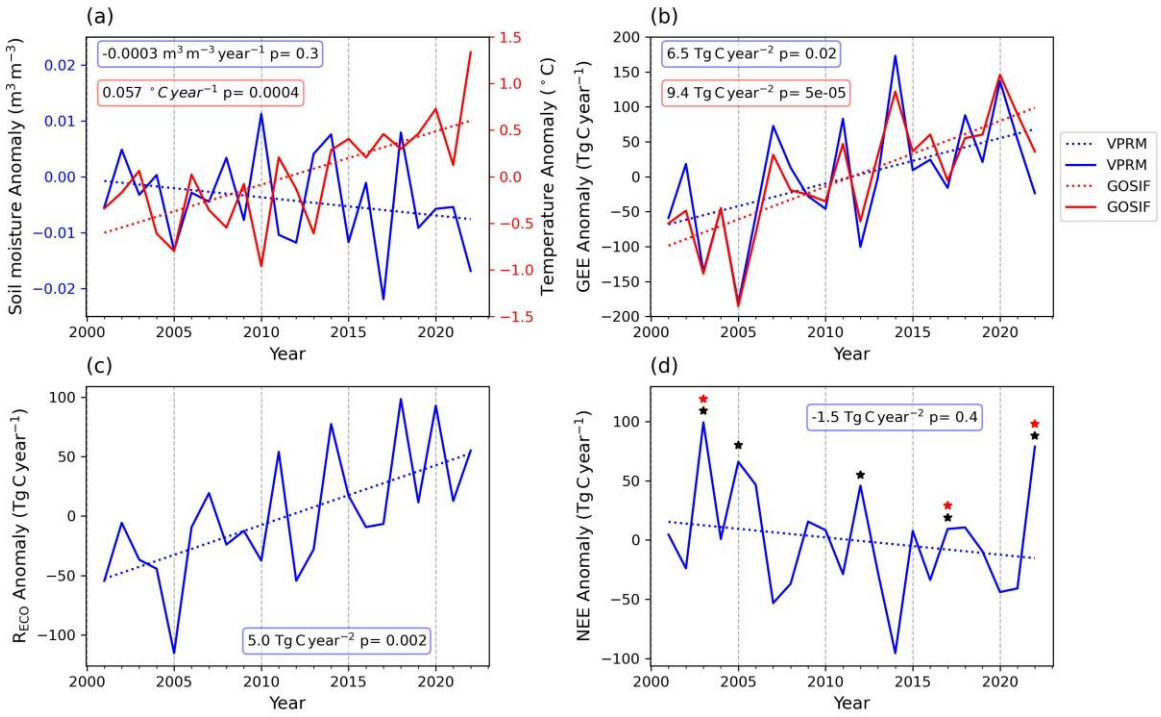

Figure 4. Time-series of annual anomalies over the study area. Annual anomalies in the climate data and carbon fluxes during 2001-2022. (a) soil moisture and temperature, (b) GEE, (c) R_{ECO} and (d) NEE aggregated annually over the entire study area (black box in Figure 1). The dashed lines represent the trends, while in the boxes the trends and the p value are detailed. The black stars in subplot (d) mark the years in which the SPEI aggregated over 1-, 3-, 6-, 9- or 12-months during summer is below -1, indicating a drought affecting most of the study area. The red stars mark the years when the summer temperature anomalies are above 1 °C, indicating a summer heat event.

3.2 Interannual variability of the biogenic carbon fluxes

We show in Figure 5 the correlation between GEE and R_{ECO} interannual anomalies and the SPEI aggregated over 1, 3, and 6 months (SPEI01, SPEI03 and SPEI06, respectively), and the partial correlation with the climate drivers such as air temperature (T2M), soil moisture and radiation during the growing season months at the ten biogeographical regions. Water availability prevails as the dominant driver of GEE interannual variability. Except for the Alps, the strongest correlations with GEE anomalies are found for SPEI (spatial median ranges between 0.38 and 0.76) and soil moisture (between 0.35 and 0.64). These results suggest that seasonal and extended droughts significantly influence GEE fluctuations. The correlations with SPEI at higher timescale aggregations (9 and 12 months) show lower correlations (between 0.26 and 0.73) than for lower timescale (Figure S4). Excluding the Alps, soil moisture exhibits generally significant positive partial correlations with GEE anomalies, while air temperature (between -0.28 and 0.21) shows primarily non-significant negative partial correlations. Higher temperatures during the growing season led to reduced CO_2 capture, while increased precipitation and soil moisture promote the photosynthetic activity. Although radiation presents a positive correlation with GEE, it is generally non-significant. Both GOSIF and VPRM show a good agreement across biogeographical regions and climate drivers (Figure S4), confirming that both models are able to simulate the observed interannual variability.

In semi-arid regions such as the Iberian sclerophyllous and Tyrrhenian-Adriatic regions, with low annual precipitation (< 800 mm $year^{-1}$) and early growing seasons (Figure S1), strong positive correlations are found between SPEI aggregated over 6 months and GEE anomalies (r=0.76 for IbeScl., and r=0.73 for TyrAdr.). During the growing season of low-altitude regions (excluding Alps, Apennine, and Corsican montane forests), GEE exhibits generally negative partial correlations with air temperature (between -0.28 and 0.01), while R_{ECO} shows positive partial correlations (between 0.03 and 0.40). In temperate humid regions like the Atlantic, Western Europe and Po Basin, R_{ECO} displays weaker correlations with SPEI (r= 0.12 to 0.42) compared to GEE (SPEI: r= 0.37 to 0.61), indicating that R_{ECO} is less sensitive to droughts in such regions. Conversely, in south-eastern regions like Tyrrhenian-Adriatic, Apennine and

Corsican montane, R_{ECO} exhibits stronger correlations with SPEI and partial correlations with soil moisture (SPEI: r= 0.55 to 0.81; SM2: r= 0.61 to 0.79)

Annually-aggregated GEE anomalies show similar patterns with drought indices and climate drivers (Figure S5), including SPEI and soil moisture, but weaker absolute values (SPEI: 0.14-0.60; SM2: 0.24-0.52), suggesting that climate driver strength throughout the year has a smaller impact on annual anomalies compared to the growing season. However, excluding Alps, Apennine and Corsican montane forests, annual aggregate GEE anomalies display higher positive correlations with air temperature (between 0.00 and 0.28), indicating that off-season temperature increases enhance gross carbon capture. In high-altitude regions, the partial correlations of annual temperature and GEE anomalies are lower (between 0.09 and 0.40) than during the growing season months (between 0.21 and 0.44).

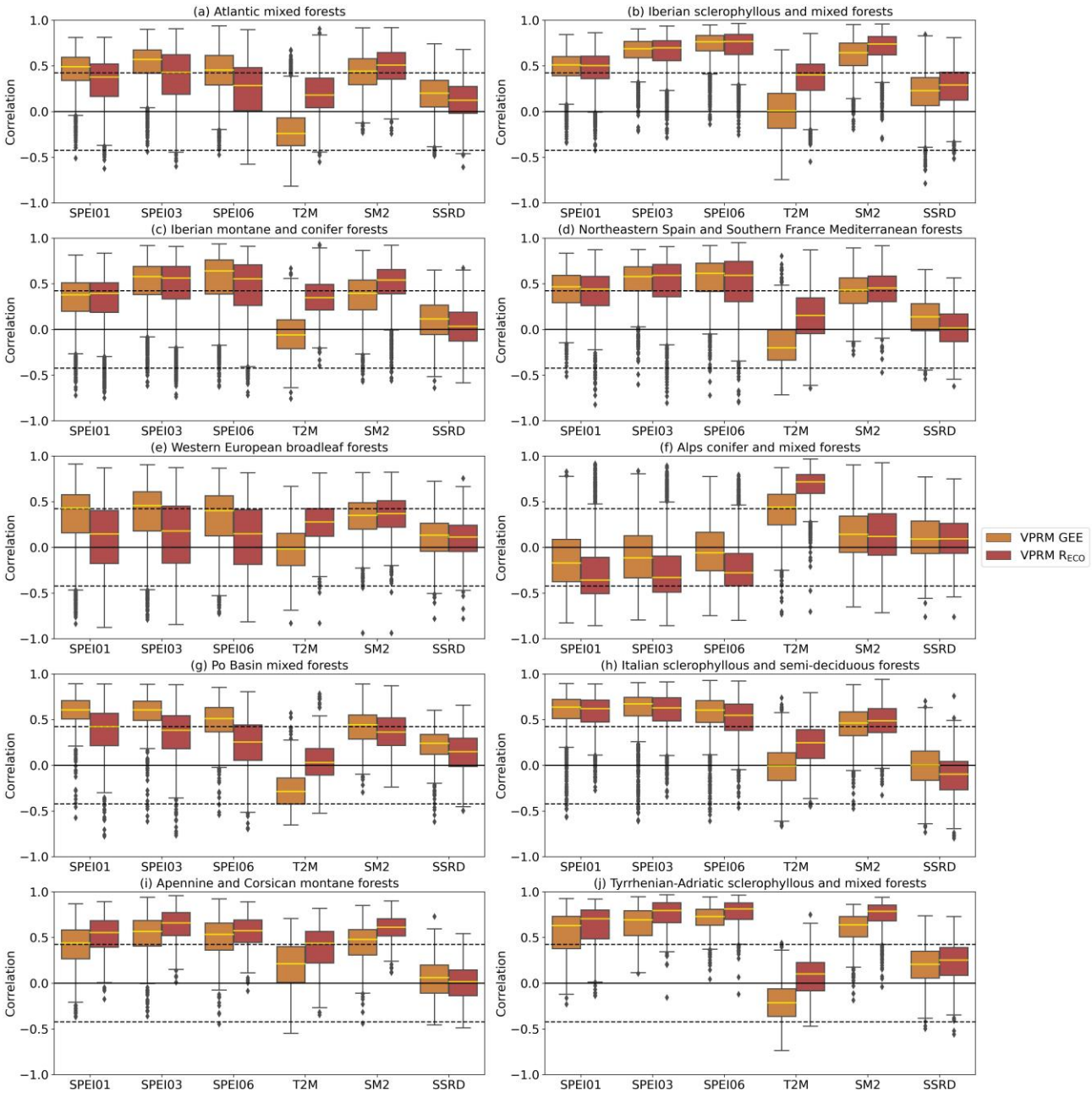
(a) Atlantic mixed forests
(b) Iberian sclerophyllous and mixed forests
(c) Iberian montane and conifer forests
(d) Northeastern Spain and Southern France Mediterranean forests
(e) Western European broadleaf forests
(f) Alps conifer and mixed forests
(g) Po Basin mixed forests
(h) Italian sclerophyllous and semi-deciduous forests
(i) Apennine and Corsican montane forests
(j) Tyrrhenian-Adriatic sclerophyllous and mixed forests
Correlation
1.0
0.5
0.0
−0.5
−1.0
SPEI01
SPEI03
SPEI06
T2M
SM2
SSRD
VPRM GEE
VPRM R_{ECO}

367

Figure 5. Interannual drivers of carbon flux anomalies. Boxplots of correlation values between GEE and RECO detrended anomalies and the different climate drivers and drought indices aggregated over all the year for each biogeographical region. The median is represented with a yellow line. The discontinuous black lines represent the limit when correlations are significant ($p<0.05$). T2M: 2 m temperature. SM2: soil moisture between 7 and 28 cm depth. SSRD: surface solar radiation downwards.

We analyse the correlation between SPEI and GEE anomalies for the biogeographical regions displaying significant trends (Figure 6, see Supporting information, Figure S6 for the rest). This time-lagged analysis covers the summer season in the same year (0 months), spring in the same year (-3 months), and so forth, up to autumn two years before the growing season (-21 months). Generally, strong, and significant correlations exist between SPEI and GEE anomalies during the growing season in the same year, gradually decreasing with earlier seasons. An exception occurs in the Alps (Figure 6f), where SPEI displays a negative non-significant correlation in the same year's summer and spring, with the correlation increasing in the preceding seasons until the previous autumn. In humid temperate regions like the Atlantic and Western Europe, correlations decrease faster over time, becoming non-significant before the summer season. We observe in these humid regions that correlations decrease much faster over the previous seasons for R_{ECO} than for GEE (Figure S7). This is different from the Mediterranean climate regions, such as Iberian and Tyrrhenian-Adriatic sclerophyllous, where significant correlations persist even for the previous spring (-3 months) or winter (-6 months), both for GEE and R_{ECO}. In these two regions, GEE anomalies exhibit a stronger correlation with short-time scale droughts (SPEI01 and SPEI03) occurring during the spring than during the summer.

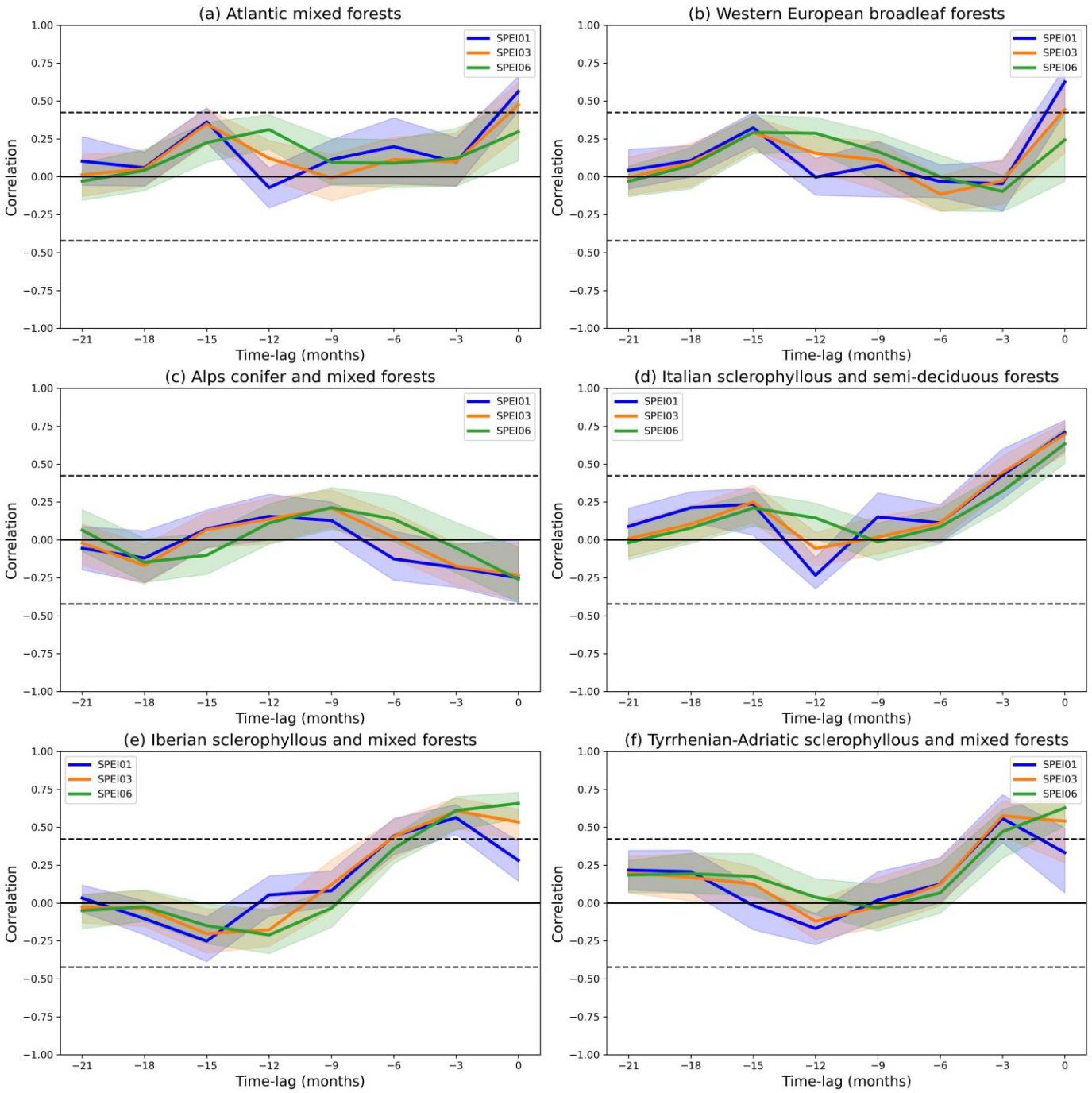

Figure 6. Correlogram between SPEI and GEE anomalies. Correlogram between the growing season anomaly in the GEE and the SPEI aggregated at 1 month (blue), 3 months (orange) and 6 months (green) averaged over the time-lagged previous seasons. 0 months represent the SPEI between June to August of the same year, -3 months the SPEI between March to May of the same year, and so on, until -21 months represent the SPEI between September to November of two years before the growing season. The bold lines represent the median correlation between all

the grid cells inside the biogeographical region, and the shaded areas represent the interquartile range.

In the case of the NEE (Figure 7), we observe that for humid regions like the Atlantic and Western Europe, the correlation pattern is similar to the GEE but in opposite sign. However, in Mediterranean climate regions, such as Iberian and Tyrrhenian-Adriatic sclerophyllous, the correlations between NEE anomalies and droughts during summer, spring and winter are much lower in absolute value than for the GEE.

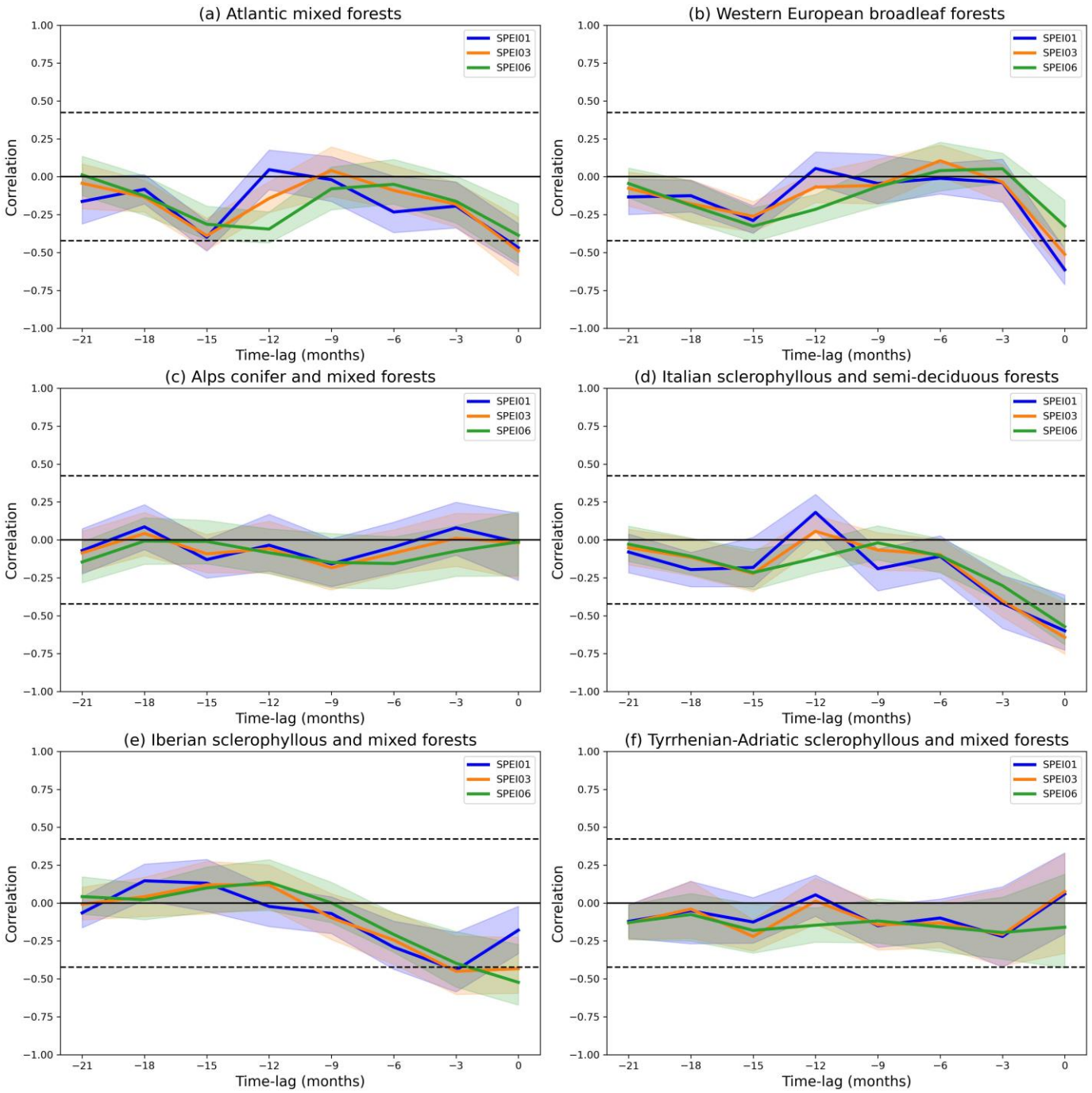

Figure 7. Correlogram between SPEI and NEE anomalies. As Figure 6 but for NEE anomalies.

3.3 Intra-annual variability of the biogenic carbon fluxes

In the following section we study the intra-annual variability of the biogenic carbon fluxes for three study cases. Figure 8a presents the temporal evolution of the biogenic flux anomalies inside the Western Europe region in 2003. The model indicates reduced GEE from June to September, reaching a minimum of -3.2 ± 1.7 g C $m^{-2}day^{-1}$ (the error corresponds to spatial standard deviation) in early August. R_{ECO} also shows a negative anomaly during summer, albeit smaller than GEE, reaching only -1.3 ± 0.8 g C $m^{-2}day^{-1}$. The region experienced low soil moisture from March to September, exacerbated by high summer temperatures, especially during a heat wave in August (+8 °C). This affected considerably the GEE and the NEE, presenting the lowest values in the moment of maximum soil moisture anomaly, and turning the ecosystems in the region from net carbon sinks into net carbon sources (Figure S8). The negative anomalies during summer were partially offset by an increase in April, May, and June, linked to positive air temperature anomalies (Figure 8d). The drought event of 2003 caused a 20.4 Tg C $year^{-1}$ (-38.8 %) reduction in net carbon capture in Western Europe region. The Atlantic, Po Basin, and Italian sclerophyllous regions were also severely affected (Figure S9), with respective annual NEE reductions of 11.5 Tg C $year^{-1}$ (-15.9 %), 7.8 Tg C $year^{-1}$ (-85.4 %) and 10.2 Tg C $year^{-1}$ (-40.8 %). Across the entire domain (Figure 1), the year 2003 had a net carbon loss of 99.6 Tg C $year^{-1}$ (-34.1 %).

Figure 8b depicts the impact of the 2005 drought on biogenic carbon fluxes in the Iberian sclerophyllous region. VPRM indicates reduced GEE and R_{ECO} from late January to October. Higher GEE reductions appear in late April and May (-1.9 ± 1.0 g C $m^{-2}day^{-1}$). GEE and R_{ECO} anomalies evolve similarly, although the impact on the R_{ECO} is lower (-1.6 ± 0.7 g C $m^{-2}day^{-1}$). Climate driver anomalies (Figure 8e) reveal persistent negative soil moisture anomalies, dipping to -0.08 m^3m^{-3} from the start of the year to October, particularly during spring when fluxes are lowest. Negative temperature anomalies (below -5 °C) were observed during winter, delaying the beginning of the growing season, while May-July featured positive temperature anomalies (> 3 °C), further depleting soil moisture. The event led to a 64.9 Tg C $year^{-1}$ (-25.0 %) reduction in annual GEE, and 47.1 Tg C $year^{-1}$ (-18.6 %) decrease in annual R_{ECO}, resulting in a 17.8 Tg C $year^{-1}$ (-281.4 %) NEE decrease. The Atlantic, Iberian montane, north-eastern Spain and southern France regions also experienced NEE reductions (Figure S10) of 11.0 Tg C $year^{-1}$ (-15.2 %), 6.5 Tg C $year^{-1}$ (-35.4 %) and 3.2 Tg C $year^{-1}$ (-17.9 %), respectively. In the south-western European region, the 2005 drought caused a total reduction of 66.5 Tg C $year^{-1}$ (-22.8 %).

In 2022, south-western Europe experienced its hottest recorded summer, coupled with an extended drought event extending from winter until November (Copernicus Climate Change Service (C3S), 2023). Winter and spring precipitation and soil moisture deficits further increased during summer due to the unusual warmer temperatures and multiple heat wave episodes (Copernicus Climate Change Service (C3S), 2023). Figure 8c shows the 2022 spatial mean GEE and R_{ECO} anomalies in the Atlantic region. GEE remains persistently low from June to August, except for early July. R_{ECO} also showed negative summer anomalies, although for a shorter period and with smaller reductions than GEE. During spring, GEE and R_{ECO} experienced positive anomalies (over 2.1 ± 0.9 g C $m^{-2}day^{-1}$), driven by the exceptionally high temperatures during May (over +4 °C) (Figure 8f). The VPRM model estimates an annual decrease of the net carbon capture of 13.8 Tg C $year^{-1}$ (-19.1 %) in the region and 78.5 Tg C $year^{-1}$ (-26.9 %) in the south-western European domain.

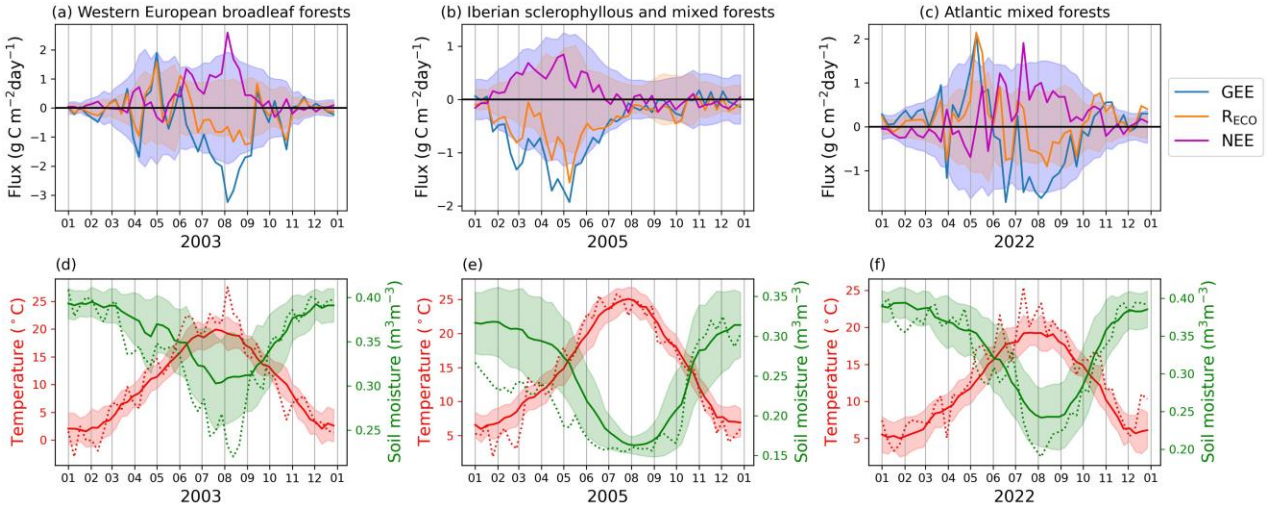

Figure 8. Intra-annual impact of heat and droughts. Time series of the spatially average anomalies for the Western European in 2003 (a,d), Iberian sclerophyllous in 2005 (b,e), and Atlantic mixed forest in 2022 (c,f) for (a,b,c) 8-daily GEE (blue), R_{ECO} (orange) and NEE (pink). (d,e,f) spatially averaged 8-daily 2 m temperature (red) and soil moisture in the 7-28 cm depth layer (green) for the study year (dotted line) and the climatic mean for the 2001 to 2022 period (solid line). The shaded areas correspond to the temporal standard deviation for each 8-daily period.

4 Discussion

4.1 Long-term trends of the biogenic carbon fluxes

In this study, we analysed the long-term trends and interannual variability of biogenic carbon fluxes in the south-western European region from 2001 to 2022, to understand the response of these fluxes to heat and drought events. The statistical analysis of the biogenic carbon fluxes reveals an overall increase or stability of GEE (spatial median of 5.51 g C m^{-2} $year^{-2}$ for GOSIF and 3.75 g C m^{-2} $year^{-2}$ for VPRM) and R_{ECO} (3.06 g C m^{-2} $year^{-2}$ for VPRM). These trends are particularly prominent in spring and in montane regions like the Alps, Apennines, Pyrenees, and Dinaric Alps. We identify a positive trend of the enhanced vegetation index (EVI) derived from MODIS surface reflectances (Vermote, 2015) over the Mediterranean region (trends up to 0.0014 EVI $year^{-1}$) which is more evident during the spring and winter months (Figure S11). Additionally, when examining long-term trends in the air temperatures using ERA5-Land data (Muñoz-Sabater, 2019) (Figure S12), a more substantial winter warming (up to 0.2 °C $year^{-1}$) is observed over these same regions. The temperature rise during the colder season contributes to the increase in GEE and R_{ECO} values by alleviating growth limitations and extending the growing season (Keenan et al., 2016). This is supported by similar increases in the GOSIF dataset, which relies solely on SIF satellite data (Li & Xiao, 2019), reinforcing the notion of elevated carbon capture in high-altitude regions of the south-western European region.

However, differences between GOSIF and VPRM are observed in other biogeographical regions, possibly due to differences in model parameterization and input data. The discrepancies between the two models impairs our ability to conclude about the long-term trends in NEE. GOSIF exhibits overall a higher spatial median compared to VPRM. GOSIF solely relies on SIF data and an ensemble of SIF-GEE linear relationships computed from global flux tower data, whereas VPRM combines remotely sensed vegetation indices, meteorological data, and region-specific model parameters. Consequently, the long-term increase in GOSIF is directly linked to SIF data, whereas VPRM's response is influenced by both vegetation indices and climate drivers. The higher sensitivity of VPRM to interannual climate variations explains the lower

extension of areas with a significant long-term trend. Additionally, VPRM is more responsive to higher temperatures during the growing season (Figure S12), particularly in summer and autumn, and the decrease in the soil moisture (Figure S13), over the south-western Iberian Peninsula and the Central Massif of France.

According to VPRM simulations, long-term trends indicate that R_{ECO} has also increased in the past two decades, at a slower rate than GEE but affecting a larger area (see Figure 2). The increase in R_{ECO}, especially in high-altitude regions, partially offsets the increase in GEE, resulting in only a modest increase in the NEE carbon sink (0.80 g C m^{-2} $year^{-2}$). This balance suggests that the south-western Europe ecosystems maintain equilibrium between increased carbon uptake through photosynthesis and carbon released through respiration. Unlike temperate and boreal forests, which are experiencing a long-term increase of their carbon sink potential (Yang et al., 2023; Yu et al., 2022), the Mediterranean regions exhibits balanced long-term carbon cycle trends. Ongoing warming and drying trends in the region may lead to uncompensated responses in GEE and R_{ECO}, causing variations in the NEE trends. For instance, we have identified a positive trend in NEE of croplands in the Central Massif of France (Figure 3e) coinciding spatially with a drying trend in the region (Figure S13) (X. Liu et al., 2021). These prospects could further compromise the net carbon sink capacity of other agricultural ecosystems in south-western Europe as the ongoing drying trend (Figure 4a) continues and affects other regions in the domain. These findings highlight the vulnerability of the south-western European region's carbon sink capacity to potential shifts in carbon flux trends, especially under the influence of more frequent and intense droughts.

4.2 Heat and drought events control the interannual variability of the fluxes

The analysis of the interannual variability in biogenic carbon fluxes emphasizes the significant influence of climatic drivers on the detrended anomalies of these fluxes. Across all the biogeographical regions, except for the Alps ecosystems, water availability emerges as the dominant climatic driver for interannual variabilities (see Figure 5). This is evident through the strong correlation observed between these fluxes and both soil moisture and the SPEI. The close agreement between VPRM and GOSIF correlations further supports the influence of soil moisture and SPEI on GEE variability. This alignment is notable, considering that initially, one might attribute this relationship to soil moisture as a driver of the VPRM model.

Analysing the influence of climate drivers on GEE reveals a direct link between climate dryness and the extent to which droughts influence the interannual variabilities of GEE. The regions where the water balance plays a more important role on the interannual anomalies of the GEE during the growing season are the semi-arid regions of the Iberian and Tyrrhenian-Adriatic sclerophyllous and mixed forests (see Figure 5). In these regions, GEE is strongly correlated with the occurrence of droughts during the growing season and in the previous six months (from the previous autumn forward). These findings align with previous research by Gouveia et al. (2017), who noted that, during the month of May, Mediterranean dry vegetation communities present the highest correlations between the vegetation activity and the SPEI aggregated at time scales between 3 and 9 months, which are associated with croplands. These regions have a high extension of non-forest vegetation (more than 85 % of the vegetated areas) and the lowest annual precipitation among the studied biogeographical regions (less than 800 mm), explaining the heightened sensitivity to soil moisture availability during periods of active vegetation growth (Vicente-Serrano, 2007). In contrast, the Alps, characterized by the lowest annual temperatures (3.8°C) and the highest precipitation levels (1485 mm) in the study area, exhibit a positive correlation with air temperature and negative correlations with SPEI and soil moisture. This pattern suggests that the Alps' vegetation faces continuous energy limitations. Warmer temperatures and increased solar radiation tend to bring climatic conditions closer to the optimal temperatures for photosynthesis (between 18 and 22 °C), while regional droughts have a relatively lower impact on the water availability of the region.

While increased air temperatures negatively impact GEE anomalies (except for the Alps), their impact on the R_{ECO} is less pronounced. These differences can be attributed to distinct ecophysiological responses of photosynthesis and respiration to temperature and soil moisture stress. Air temperature impacts the photosynthesis when it surpasses a certain optimum temperature by reducing the chemical reaction kinetics (von Buttlar et al., 2018), whereas soil moisture stress impacts photosynthesis by ecophysiological and structural changes (Bréda et al., 2006). On the other hand, increasing soil temperatures, and hence air temperatures, stimulates heterotrophic respiration by increasing the kinetics of soil microbial decomposition, root respiration and the diffusion of enzymes (von Buttlar et al., 2018), while strong soil moisture deficits produced by droughts affects negatively the soil microbial activity and reduces autotrophic respiration due to the reduction of recently assimilated carbon (Migliavacca et al.,

2011; Reichstein et al., 2003). Therefore, while an increase of temperature during the growing season can be negative for the photosynthesis, especially if it is accompanied by a drought, the impact on the ecosystem respiration is reduced by the compensating effects. It is worth noting that these responses vary depending on the ecosystem and vegetation species.

Our analysis reveals a higher influence of droughts on GEE anomalies compared to R_{ECO} anomalies in temperate humid regions like the Atlantic, Western Europe, and the Po Basin regions. In contrast, the impacts of droughts on GEE and R_{ECO} in other Mediterranean climate regions show similar correlations. The different responses of GEE and R_{ECO} to drought occurrences between humid and dry climates may be attributed to various factors, including higher intra-annual compensation effect for R_{ECO} compared to GEE in humid regions, the resistance capacity of Mediterranean vegetation to seasonal droughts (Gazol et al., 2018), and lagged responses of R_{ECO} to drought compared to more immediate effects on GEE **(Ryan & Law, 2005)**. These findings align with previous studies on the 2003 summer drought and heat event in Central Europe (Ciais et al., 2005; Reichstein et al., 2007), which reported a higher impact of drought on GEE compared to R_{ECO} in temperate ecosystems. We note that temperate humid regions exhibit the highest net carbon sink in the study area (see Figure S14) but also higher nonlinearities in the response of GEE and R_{ECO} to drought occurrence during the growing season. Consequently, anomalies in NEE are highly influenced by droughts in these regions compared to Mediterranean regions (Figure S15). These results emphasize the vulnerability of the south-western Europe's net carbon sink to drought occurrences.

4.3 Warm springs do not compensate the decreasing effect of droughts on CO_2 fluxes

We find that both GEE and R_{ECO} decrease during the summer for Western European broadleaf forests in 2003 and the Atlantic mixed forests in 2022, revealing similar impact of heat and water stress on the ecosystem carbon fluxes. This can be explained by the heat wave in conjunction with persistent drought conditions (Bastos et al., 2014; García-Herrera et al., 2010) as shown by several studies on the coupled effects of heat and water stress on the photosynthetic capacity of Mediterranean ecosystems (Bastos et al., 2014; Ciais et al., 2005; Ermitão et al., 2021; Reichstein et al., 2007).

However, the impact of heat-drought combined conditions on R_{ECO} is lower than for GEE. Moreover, the impact on the R_{ECO} seems to be lagged with respect to the GEE, starting to stress between 8 and 16 days after the stress is observed in the GEE, while recovering concurrently to the GEE once the heat and water stress subsided. These differential responses between GEE and R_{ECO} resulted in a reduction of the net carbon capture capacity of the ecosystems and turning ecosystems from net carbon sinks to carbon sources (see Figure S8). These results align with the ones obtained by (von Buttlar et al., 2018), who found from eddy-covariance flux measurements that the combination of drought and heat typically led to a strong decrease in GEE, whereas heat and drought impacts on respiration partially offset each other.

For the 2003 and 2022 study cases, we find that the impact of summer heat and drought events are partially compensated by abnormally warm temperatures between April and June, which led to an increase in GEE and R_{ECO}. The impact of the warm spring temperatures produced similar positive anomalies in magnitude on the GEE and R_{ECO}. The high spring R_{ECO} anomaly detected in these two study cases could be attributed to the combination of high spring temperatures and the high GEE anomalies at the peak of the growing season, causing an increment of the recently assimilated carbon to respire. The similar increment of the GEE and R_{ECO} during spring compensates each other, resulting in a minimal NEE anomaly during the spring.

These distinct seasonal compensation effects between spring and summer led to an overall reduction in NEE compared to normal values during the growing season, dominating the anomalies for the entire year. These findings highlight the importance of studying the combined impacts of heat and drought events on both GEE and R_{ECO}, as they can cause non-linear effects on the terrestrial carbon balance. Focusing solely on GEE might underestimate the true impact of heat and drought events on ecosystems, and the terrestrial carbon balance.

These results suggests that the Mediterranean ecosystems, adapted to recurrent seasonal droughts during the summer (Peñuelas & Sardans, 2021), are more vulnerable to the occurrence of persistent soil moisture deficits at the beginning of the growing season, especially if persistent drought conditions affect the previous humid seasons. The Iberian sclerophyllous region is principally cultivated with winter crops (Gouveia et al., 2017), which can be affected by water deficits at early stages of crop development. Moreover, the cold winter conditions during 2005 in the Iberian Peninsula (anomalies of -5°C) may have also affected GEE by delaying the beginning

608 of the growing season or with a direct frost damage. These results highlight the potential
609 recurrent stress that will suffer the Iberian ecosystems under future climate scenarios, and the
610 compromised carbon balance from these ecosystems (Moemken et al., 2022).
611

612 **4.4 VPRM modifications improve the response of the fluxes to heat and drought**

613 We modified the data-driven biosphere model VPRM for GEE and R_{ECO}
614 parameterizations, incorporating plant functional type-specific parameters calibrated using data
615 solely from flux tower stations in the southern Europe and neighbouring regions. These
616 modifications include the inclusion of soil moisture-related water stress in the GEE
617 parameterization (Fu et al., 2022), resulting in improved model GEE estimates that better align
618 with changes between energy and water-limited regimes. This modification improves the
619 correlation between modelled-predicted and observed weekly GEE estimates in evergreen-leaf
620 ecosystems, such as Mediterranean evergreen forests (cf. Supporting information). Additionally,
621 we implemented a more sophisticated semi-empirical R_{ECO} parameterization that considers
622 vegetation productivity (GEE) and soil moisture, enhancing the predictive capability of the
623 model to analyse seasonal and annual variations of the carbon balance (Migliavacca et al., 2011).

624 However, several limitations emerge from the VPRM model for long-term biogenic flux
625 studies. For instance, the VPRM model relies on a land cover map based on the Synergetic Land
626 Cover Product (SYNMAP) (Jung et al., 2006), which joins three global land cover products
627 based on satellite observations as recent as 2001, failing to account land-use/land-cover changes
628 during the 2001 to 2022 period. This limitation could be solved by incorporating dynamic land-
629 cover maps as the MODIS MCD12Q1 product (Friedl & Sulla-Menashe, 2019). Moreover, the
630 application of static parameters for each PFT for the 2001 to 2022 period could not properly
631 capture the increase in the light-use-efficiency factor due to the atmospheric CO_2 fertilization
632 effect (Keenan et al., 2016). A dynamic set of VPRM parameters, updated every few years, could
633 address this issue, provided a continuous and standardized dataset of carbon flux tower
634 observations encompassing various biogeographical regions, climates and PFT becomes
635 available. Despite the commendable efforts of organizations like FLUXNET (Pastorello et al.,
636 2020) and the Integrated Carbon Observation System (ICOS), certain biomes and PFT remain
637 underrepresented in observation datasets, as it is the case of the croplands in semi-arid regions of

638 the Iberian, Tyrrhenian, and Adriatic sclerophyllous regions. This underrepresentation
639 contributes to model uncertainties in estimating biogenic fluxes in these regions. The VPRM
640 predicting capabilities and the analysis of the carbon balance would benefit from the
641 incorporation of novel flux tower sites in these underrepresented biomes and PFT.

642 Despite the enhancements made to the R_{ECO} parameterization, the model evaluation
643 reveals moderate correlations with R_{ECO} observations, compared to GEE and NEE (Figure S18,
644 in Supporting information). This discrepancy suggests the existence of unaccounted processes
645 within the model. These processes could relate to carbon pool size (Reichstein et al., 2003), the
646 maximum leaf area index throughout the year, nitrogen deposition, and stand age (Migliavacca et
647 al., 2011) in natural ecosystems. In the case of croplands, factors like management practices and
648 soil carbon pools could potentially influence respiration (Eugster et al., 2010). Addressing these
649 aspects could improve R_{ECO} estimation but may introduce additional sources of model
650 uncertainty due to increased complexity. Overcoming these sources of uncertainty may be
651 possible through regional-scale inverse analysis of the CO_2 budget (Mahadevan et al., 2008),
652 leveraging atmospheric CO_2 concentration observations from towers in south-western Europe
653 (Kountouris et al., 2018; Munassar et al., 2022).

654 **5 Conclusions**

655 Using a modified VPRM model with parameters optimized for south-western Europe
656 ecosystems, this study analysed the long-term trends and interannual variability of carbon fluxes
657 in south-western Europe from 2001 to 2022, to understand the response of these fluxes to heat
658 and drought events. Our results revealed high spatial variations of the carbon fluxes trends, being
659 higher over mountainous regions in the Alps, Apennine, and Corsican montane forests. The
660 similar increases of the ecosystem's photosynthesis and respiration compensate each other,
661 resulting in only a modest increase of 0.80 g C m^{-2} $year^{-2}$ (spatial median) in net carbon capture
662 over the region. Ongoing warming and drying trends in the region may lead to uncorrelated
663 responses in gross ecosystem exchange and ecosystem respiration, causing variations in the net
664 ecosystem exchange trends. These findings highlight the vulnerability of the south-western
665 Europe's carbon sink capacity to potential shifts in carbon flux trends, especially under the
666 influence of more frequent and intense droughts.

667 Analysing the influence of climate drivers on the gross ecosystem exchange and
668 respiration reveals a direct link between climate dryness and the extent to which droughts

influence the interannual variabilities of the carbon fluxes. The regions where the water balance plays a more important role on the interannual anomalies of the gross ecosystem exchange and respiration during the growing season are the semi-arid regions of the Iberian and Tyrrhenian-Adriatic sclerophyllous regions. These regions, contrary to the other regions, present a higher influence of droughts on the gross ecosystem exchange variability during the spring, rather than on summer. However, this analysis reveals a higher influence of droughts on gross ecosystem exchange anomalies compared to ecosystem respiration anomalies in temperate humid regions like the Atlantic, Western Europe, and the Po Basin. We show here that temperate humid regions exhibit the highest net carbon sink in our study area but also display highly nonlinear responses of the carbon fluxes to drought occurrence during the growing season. Consequently, anomalies in net ecosystem exchange are highly influenced by droughts in these regions compared to Mediterranean regions. These results emphasize the vulnerability of the south-western Europe's net carbon sink capacity to drought occurrences. Additionally, we observed that the impact of summer heat and drought events reduces the net carbon capture, even turning ecosystems from carbon sinks to carbon sources, while we did not observe intra-annual compensations from the preceding warm spring due to compensating increases in gross ecosystem exchange and respiration. These findings emphasize the importance of studying the combined impacts of heat and drought events on both ecosystem photosynthesis and respiration, as they can cause non-linear impacts on the terrestrial carbon balance.

Acknowledgments

This work has been made possible thanks to the financial support of the European Research Council (ERC) Consolidator project: Integrated System Analysis of Urban Vegetation and Agriculture (818002-URBAG), the Spanish Ministry of Science, Innovation and Universities, Through the "Maria de Maeztu" programme for Units of Excellence (CEX2019-000940-M), and the funding and recognition awarded to research group Sostenipra (2021 SGR 00734) by the Department of Research and Universities of the Generalitat de Catalunya. The authors thankfully

acknowledge the computer resources at PICASSO and the technical support provided by the Universidad de Málaga (RES-AECT-2020-2-0004). This work used eddy covariance data acquired and shared by the FLUXNET community, including these networks: AmeriFlux, AfriFlux, AsiaFlux, CarboAfrica, CarboEuropeIP, CarboItaly, CarboMont, ChinaFlux, Fluxnet-Canada, GreenGrass, ICOS, KoFlux, LBA, NECC, OzFlux-TERN, TCOS-Siberia, and USCCC. The FLUXNET eddy covariance data processing and harmonization was carried out by the ICOS Ecosystem Thematic Center, AmeriFlux Management Project and Fluxdata project of FLUXNET. The authors also thank the ICOS Infrastructure for support in collecting and curating the flux tower data. The authors also acknowledge the Drs. Jingfeng Xiao and Xing Li research group for the GOSIF GEE data. T. Lauvaux was supported by the French National Chair program Carbon Across Scales and Landscapes (CASAL).

Open Research

The VPRM version with the modifications detailed in this study are available in a Python program in the repository "Vegetation Photosynthesis and Respiration Model code and output for south-western Europe between 2001 and 2022" at Zenodo, via https://doi.org/10.5281/zenodo.10782550 with Creative Commons Attribution 4.0 International license (Villalba, 2024). In this repository there are also the terrestrial ecosystem carbon fluxes estimated with the modified VPRM over the south-western Europe domain between 2001 and 2022 used in this study in NetCDF format. The hourly ERA5-Land data (Muñoz-Sabater, 2019) was downloaded from the Copernicus Climate Change Service (C3S) Climate Data Store (2022). Neither the European Commission nor ECMWF is responsible for any use that may be made of

the Copernicus information or data it contains. The MODIS MOD09A1 v6.1 product used for deriving the remotely-sensed vegetation indices in this study are available at the NASA EOSDIS Land Processes Distributed Active Archive Center via https://doi.org/10.5067/MODIS/MOD09A1.061.

References

Barriopedro, D., Fischer, E. M., Luterbacher, J., Trigo, R. M., & García-Herrera, R. (2011). The hot summer of 2010: Redrawing the temperature record map of Europe. *Science*, *332*(6026). https://doi.org/10.1126/science.1201224

Bastos, A., Ciais, P., Friedlingstein, P., Sitch, S., Pongratz, J., Fan, L., Wigneron, J. P., Weber, U., Reichstein, M., Fu, Z., Anthoni, P., Arneth, A., Haverd, V., Jain, A. K., Joetzjer, E., Knauer, J., Lienert, S., Loughran, T., McGuire, P. C., … Zaehle, S. (2020). Direct and seasonal legacy effects of the 2018 heat wave and drought on European ecosystem productivity. *Science Advances*, *6*(24). https://doi.org/10.1126/sciadv.aba2724

Bastos, A., Gouveia, C. M., Trigo, R. M., & Running, S. W. (2014). Analysing the spatio-temporal impacts of the 2003 and 2010 extreme heatwaves on plant productivity in Europe. *Biogeosciences*, *11*(13), 3421–3435. https://doi.org/10.5194/bg-11-3421-2014

Bréda, N., Huc, R., Granier, A., & Dreyer, E. (2006). Temperate forest trees and stands under severe drought: a review of ecophysiological responses, adaptation processes and long-term consequences. *Annals of Forest Science*, *63*(6), 625–644. https://doi.org/10.1051/forest:2006042

Ciais, P., Reichstein, M., Viovy, N., Granier, A., Ogée, J., Allard, V., Aubinet, M., Buchmann, N., Bernhofer, C., Carrara, A., Chevallier, F., De Noblet, N., Friend, A. D., Friedlingstein, P., Grünwald, T., Heinesch, B., Keronen, P., Knohl, A., Krinner, G., … Valentini, R. (2005). Europe-wide reduction in primary productivity caused by the heat and drought in 2003. *Nature*, *437*(7058), 529–533. https://doi.org/10.1038/nature03972

Ciais, P., Tan, J., Wang, X., Roedenbeck, C., Chevallier, F., Piao, S.-L., Moriarty, R., Broquet, G., Le Quéré, C., Canadell, J. G., Peng, S., Poulter, B., Liu, Z., & Tans, P. (2019). Five

747 decades of northern land carbon uptake revealed by the interhemispheric CO2 gradient.
748 *Nature*, *568*(7751), 221–225. https://doi.org/10.1038/s41586-019-1078-6
749 Copernicus Climate Change Service (C3S). (2022). ERA5-Land hourly data from 1950 to
750 present [dataset]. Copernicus Climate Change Service (C3S) Climate Data Store (CDS).
751 https://doi.org/10.24381/CDS.68D2BB30 (Accessed on 24-Nov-2022).
752 Copernicus Climate Change Service (C3S). (2023). European State of the Climate 2022.
753 Copernicus Climate Change Service (C3S). https://doi.org/10.24381/GVAF-H066
754 Dayalu, A., Munger, J. W., Wofsy, S. C., Wang, Y., Nehrkorn, T., Zhao, Y., McElroy, M. B.,
755 Nielsen, C. P., & Luus, K. (2018). Assessing biotic contributions to CO2 fluxes in northern
756 China using the Vegetation, Photosynthesis and Respiration Model (VPRM-CHINA) and
757 observations from 2005 to 2009. *Biogeosciences*, *15*(21), 6713–6729.
758 https://doi.org/10.5194/bg-15-6713-2018
759 Ermitão, T., Gouveia, C. M., Bastos, A., & Russo, A. C. (2021). Vegetation Productivity Losses
760 Linked to Mediterranean Hot and Dry Events. *Remote Sensing*, *13*(19), 4010.
761 https://doi.org/10.3390/rs13194010
762 Eugster, W., Moffat, A. M., Ceschia, E., Aubinet, M., Ammann, C., Osborne, B., Davis, P. A.,
763 Smith, P., Jacobs, C., Moors, E., Le Dantec, V., Béziat, P., Saunders, M., Jans, W.,
764 Grünwald, T., Rebmann, C., Kutsch, W. L., Czerný, R., Janouš, D., … Buchmann, N.
765 (2010). Management effects on European cropland respiration. *Agriculture, Ecosystems &*
766 *Environment*, *139*(3), 346–362. https://doi.org/10.1016/j.agee.2010.09.001
767 Faranda, D., Pascale, S., & Bulut, B. (2023). Persistent anticyclonic conditions and climate
768 change exacerbated the exceptional 2022 European-Mediterranean drought. *Environmental*
769 *Research Letters*, *18*(3). https://doi.org/10.1088/1748-9326/acbc37
770 Fernández-Martínez, M., Peñuelas, J., Chevallier, F., Ciais, P., Obersteiner, M., Rödenbeck, C.,
771 Sardans, J., Vicca, S., Yang, H., Sitch, S., Friedlingstein, P., Arora, V. K., Goll, D. S., Jain,
772 A. K., Lombardozzi, D. L., McGuire, P. C., & Janssens, I. A. (2023). Diagnosing
773 destabilization risk in global land carbon sinks. *Nature*, *615*(7954), 848–853.
774 https://doi.org/10.1038/s41586-023-05725-1
775 Fischer, E. M., & Schär, C. (2010). Consistent geographical patterns of changes in high-impact
776 European heatwaves. *Nature Geoscience*, *3*(6), 398–403. https://doi.org/10.1038/ngeo866

Friedl, Mark, & Sulla-Menashe, Damien. (2019). MCD12Q1 MODIS/Terra+Aqua Land Cover Type Yearly L3 Global 500m SIN Grid V006 [Dataset]. NASA EOSDIS Land Processes Distributed Active Archive Center. https://doi.org/10.5067/MODIS/MCD12Q1.006 (Accessed on 4-Mar-2024)

Muñoz-Sabater, J. (2019). ERA5-Land hourly data from 1950 to present [Dataset]. Copernicus Climate Change Service (C3S) Climate Data Store (CDS). https://doi.org/10.24381/cds.e2161bac (Accessed on 24-Nov-2022).

Fu, Z., Ciais, P., Makowski, D., Bastos, A., Stoy, P. C., Ibrom, A., Knohl, A., Migliavacca, M., Cuntz, M., Šigut, L., Peichl, M., Loustau, D., El-Madany, T. S., Buchmann, N., Gharun, M., Janssens, I., Markwitz, C., Grünwald, T., Rebmann, C., … Wigneron, J. P. (2022). Uncovering the critical soil moisture thresholds of plant water stress for European ecosystems. *Global Change Biology*, *28*(6), 2111–2123. https://doi.org/10.1111/gcb.16050

García-Herrera, R., Díaz, J., Trigo, R. M., Luterbacher, J., & Fischer, E. M. (2010). A Review of the European Summer Heat Wave of 2003. *Critical Reviews in Environmental Science and Technology*, *40*(4), 267–306. https://doi.org/10.1080/10643380802238137

Gazol, A., Camarero, J. J., Vicente-Serrano, S. M., Sánchez-Salguero, R., Gutiérrez, E., de Luis, M., Sangüesa-Barreda, G., Novak, K., Rozas, V., Tíscar, P. A., Linares, J. C., Martín-Hernández, N., Martínez del Castillo, E., Ribas, M., García-González, I., Silla, F., Camisón, A., Génova, M., Olano, J. M., … Galván, J. D. (2018). Forest resilience to drought varies across biomes. *Global Change Biology*, *24*(5), 2143–2158. https://doi.org/10.1111/gcb.14082

Gilabert, M. A., Moreno, A., Maselli, F., Martínez, B., Chiesi, M., Sánchez-Ruiz, S., García-Haro, F. J., Pérez-Hoyos, A., Campos-Taberner, M., Pérez-Priego, O., Serrano-Ortiz, P., & Carrara, A. (2015). Daily GPP estimates in Mediterranean ecosystems by combining remote sensing and meteorological data. *ISPRS Journal of Photogrammetry and Remote Sensing*, *102*, 184–197. https://doi.org/10.1016/j.isprsjprs.2015.01.017

Giorgi, F., & Lionello, P. (2008). Climate change projections for the Mediterranean region. *Global and Planetary Change*, *63*(2–3), 90–104. https://doi.org/10.1016/j.gloplacha.2007.09.005

Gourdji, S. M., Karion, A., Lopez-Coto, I., Ghosh, S., Mueller, K. L., Zhou, Y., Williams, C. A., Baker, I. T., Haynes, K. D., & Whetstone, J. R. (2022). A Modified Vegetation Photosynthesis and Respiration Model (VPRM) for the Eastern USA and Canada, Evaluated With Comparison to Atmospheric Observations and Other Biospheric Models. *Journal of Geophysical Research: Biogeosciences*, *127*(1). https://doi.org/10.1029/2021JG006290

Gouveia, C. M., Trigo, R. M., Beguería, S., & Vicente-Serrano, S. M. (2017). Drought impacts on vegetation activity in the Mediterranean region: An assessment using remote sensing data and multi-scale drought indicators. *Global and Planetary Change*, *151*, 15–27. https://doi.org/10.1016/j.gloplacha.2016.06.011

Ionita, M., Tallaksen, L. M., Kingston, D. G., Stagge, J. H., Laaha, G., Van Lanen, H. A. J., Scholz, P., Chelcea, S. M., & Haslinger, K. (2017). The European 2015 drought from a climatological perspective. *Hydrology and Earth System Sciences*, *21*(3), 1397–1419. https://doi.org/10.5194/hess-21-1397-2017

Jin, H., Vicente-Serrano, S. M., Tian, F., Cai, Z., Conradt, T., Boincean, B., Murphy, C., Farizo, B. A., Grainger, S., López-Moreno, J. I., & Eklundh, L. (2023). Higher vegetation sensitivity to meteorological drought in autumn than spring across European biomes. *Communications Earth & Environment*, *4*(1), 299. https://doi.org/10.1038/s43247-023-00960-w

Jolly, W. M., Dobbertin, M., Zimmermann, N. E., & Reichstein, M. (2005). Divergent vegetation growth responses to the 2003 heat wave in the Swiss Alps. *Geophysical Research Letters*, *32*(18), 1–4. https://doi.org/10.1029/2005GL023252

Jung, M., Henkel, K., Herold, M., & Churkina, G. (2006). Exploiting synergies of global land cover products for carbon cycle modeling. *Remote Sensing of Environment*, *101*(4), 534–553. https://doi.org/10.1016/j.rse.2006.01.020

Keenan, T. F., Prentice, I. C., Canadell, J. G., Williams, C. A., Wang, H., Raupach, M., & Collatz, G. J. (2016). Recent pause in the growth rate of atmospheric CO2 due to enhanced terrestrial carbon uptake. *Nature Communications*, *7*(1), 13428. https://doi.org/10.1038/ncomms13428

Kountouris, P., Gerbig, C., Rödenbeck, C., Karstens, U., Koch, T. F., & Heimann, M. (2018). Technical Note: Atmospheric CO2 inversions on the mesoscale using data-driven prior

uncertainties: methodology and system evaluation. *Atmospheric Chemistry and Physics*, *18*(4), 3027–3045. https://doi.org/10.5194/acp-18-3027-2018

Li, X., & Xiao, J. (2019). Mapping Photosynthesis Solely from Solar-Induced Chlorophyll Fluorescence: A Global, Fine-Resolution Dataset of Gross Primary Production Derived from OCO-2. *Remote Sensing*, *11*(21), 2563. https://doi.org/10.3390/rs11212563

Liu, W., Zhang, Z., & Wan, S. (2009). Predominant role of water in regulating soil and microbial respiration and their responses to climate change in a semiarid grassland. *Global Change Biology*, *15*(1), 184–195. https://doi.org/10.1111/j.1365-2486.2008.01728.x

Liu, X., He, B., Guo, L., Huang, L., Yuan, W., Chen, X., Hao, X., Xie, X., Zhang, Y., Zhong, Z., Li, T., & Chen, A. (2021). European Carbon Uptake has Not Benefited From Vegetation Greening. *Geophysical Research Letters*, *48*(20). https://doi.org/10.1029/2021GL094870

Los, S. O. (2013). Analysis of trends in fused AVHRR and MODIS NDVI data for 1982–2006: Indication for a CO2 fertilization effect in global vegetation. *Global Biogeochemical Cycles*, *27*(2), 318–330. https://doi.org/10.1002/gbc.20027

Lv, Y., Liu, J., He, W., Zhou, Y., Tu Nguyen, N., Bi, W., Wei, X., & Chen, H. (2023). How well do light-use efficiency models capture large-scale drought impacts on vegetation productivity compared with data-driven estimates? *Ecological Indicators*, *146*, 109739. https://doi.org/10.1016/j.ecolind.2022.109739

Mahadevan, P., Wofsy, S. C., Matross, D. M., Xiao, X., Dunn, A. L., Lin, J. C., Gerbig, C., Munger, J. W., Chow, V. Y., & Gottlieb, E. W. (2008). A satellite-based biosphere parameterization for net ecosystem CO2 exchange: Vegetation Photosynthesis and Respiration Model (VPRM). *Global Biogeochemical Cycles*, *22*(2). https://doi.org/10.1029/2006GB002735

Maselli, F., Papale, D., Puletti, N., Chirici, G., & Corona, P. (2009). Combining remote sensing and ancillary data to monitor the gross productivity of water-limited forest ecosystems. *Remote Sensing of Environment*, *113*(3), 657–667. https://doi.org/10.1016/j.rse.2008.11.008

Migliavacca, M., Reichstein, M., Richardson, A. D., Colombo, R., Sutton, M. A., Lasslop, G., Tomelleri, E., Wohlfahrt, G., Carvalhais, N., Cescatti, A., Mahecha, M. D., Montagnani, L., Papale, D., Zaehle, S., Arain, A., Arneth, A., Black, T. A., Carrara, A., Dore, S., … Van Der Molen, M. K. (2011). Semiempirical modeling of abiotic and biotic factors controlling

ecosystem respiration across eddy covariance sites. *Global Change Biology*, *17*(1), 390–409. https://doi.org/10.1111/j.1365-2486.2010.02243.x

Moemken, J., Koerner, B., Ehmele, F., Feldmann, H., & Pinto, J. G. (2022). Recurrence of Drought Events Over Iberia. Part II: Future Changes Using Regional Climate Projections. *Tellus A: Dynamic Meteorology and Oceanography*, *74*(2022), 262. https://doi.org/10.16993/tellusa.52

Molina, M. O., Sánchez, E., & Gutiérrez, C. (2020). Future heat waves over the Mediterranean from an Euro-CORDEX regional climate model ensemble. *Scientific Reports*, *10*(1), 8801. https://doi.org/10.1038/s41598-020-65663-0

Munassar, S., Rödenbeck, C., Koch, F.-T., Totsche, K. U., Gałkowski, M., Walther, S., & Gerbig, C. (2022). Net ecosystem exchange (NEE) estimates 2006–2019 over Europe from a pre-operational ensemble-inversion system. *Atmospheric Chemistry and Physics*, *22*(12), 7875–7892. https://doi.org/10.5194/acp-22-7875-2022

Nunes, L., Álvarez-González, J., Alberdi, I., Silva, V., Rocha, M., & Rego, F. C. (2019). Analysis of the occurrence of wildfires in the Iberian Peninsula based on harmonised data from national forest inventories. *Annals of Forest Science*, *76*(1), 27. https://doi.org/10.1007/s13595-019-0811-5

Olson, D. M., Dinerstein, E., Wikramanayake, E. D., Burgess, N. D., Powell, G. V. N., Underwood, E. C., D'amico, J. A., Itoua, I., Strand, H. E., Morrison, J. C., Loucks, C. J., Allnutt, T. F., Ricketts, T. H., Kura, Y., Lamoreux, J. F., Wettengel, W. W., Hedao, P., & Kassem, K. R. (2001). Terrestrial Ecoregions of the World: A New Map of Life on Earth: A new global map of terrestrial ecoregions provides an innovative tool for conserving biodiversity. *BioScience*, *51*(11), 933–938. https://doi.org/10.1641/0006-3568(2001)051[0933:TEOTWA]2.0.CO;2

Pastorello, G., Trotta, C., Canfora, E., Chu, H., Christianson, D., Cheah, Y.-W., Poindexter, C., Chen, J., Elbashandy, A., Humphrey, M., Isaac, P., Polidori, D., Reichstein, M., Ribeca, A., van Ingen, C., Vuichard, N., Zhang, L., Amiro, B., Ammann, C., … Papale, D. (2020). The FLUXNET2015 dataset and the ONEFlux processing pipeline for eddy covariance data. *Scientific Data*, *7*(1), 225. https://doi.org/10.1038/s41597-020-0534-3

Peñuelas, J., & Sardans, J. (2021). Global Change and Forest Disturbances in the Mediterranean Basin: Breakthroughs, Knowledge Gaps, and Recommendations. *Forests*, *12*(5), 603. https://doi.org/10.3390/f12050603

Qiu, R., Li, X., Han, G., Xiao, J., Ma, X., & Gong, W. (2022). Monitoring drought impacts on crop productivity of the U.S. Midwest with solar-induced fluorescence: GOSIF outperforms GOME-2 SIF and MODIS NDVI, EVI, and NIRv. *Agricultural and Forest Meteorology*, *323*. https://doi.org/10.1016/j.agrformet.2022.109038

Ramonet, M., Ciais, P., Apadula, F., Bartyzel, J., Bastos, A., Bergamaschi, P., Blanc, P. E., Brunner, D., Caracciolo di Torchiarolo, L., Calzolari, F., Chen, H., Chmura, L., Colomb, A., Conil, S., Cristofanelli, P., Cuevas, E., Curcoll, R., Delmotte, M., di Sarra, A., … Yver Kwok, C. (2020). The fingerprint of the summer 2018 drought in Europe on ground-based atmospheric CO2 measurements. P*hilosophical Transactions of the Royal Society B: Biological Sciences*, *375*(1810), 20190513. https://doi.org/10.1098/rstb.2019.0513

Reichstein, M., Bahn, M., Ciais, P., Frank, D., Mahecha, M. D., Seneviratne, S. I., Zscheischler, J., Beer, C., Buchmann, N., Frank, D. C., Papale, D., Rammig, A., Smith, P., Thonicke, K., van der Velde, M., Vicca, S., Walz, A., & Wattenbach, M. (2013). Climate extremes and the carbon cycle. *Nature*, *500*(7462), 287–295. https://doi.org/10.1038/nature12350

Reichstein, M., Ciais, P., Papale, D., Valentini, R., Running, S., Viovy, N., Cramer, W., Granier, A., Ogée, J., Allard, V., Aubinet, M., Bernhofer, C., Buchmann, N., Carrara, A., Grünwald, T., Heimann, M., Heinesch, B., Knohl, A., Kutsch, W., … Zhao, M. (2007). Reduction of ecosystem productivity and respiration during the European summer 2003 climate anomaly: A joint flux tower, remote sensing and modelling analysis. *Global Change Biology*, *13*(3), 634–651. https://doi.org/10.1111/j.1365-2486.2006.01224.x

Reichstein, M., Rey, A., Freibauer, A., Tenhunen, J., Valentini, R., Banza, J., Casals, P., Cheng, Y., Grünzweig, J. M., Irvine, J., Joffre, R., Law, B. E., Loustau, D., Miglietta, F., Oechel, W., Ourcival, J.-M., Pereira, J. S., Peressotti, A., Ponti, F., … Yakir, D. (2003). Modeling temporal and large-scale spatial variability of soil respiration from soil water availability, temperature and vegetation productivity indices. *Global Biogeochemical Cycles*, *17*(4). https://doi.org/10.1029/2003GB002035

Rita, A., Camarero, J. J., Nolè, A., Borghetti, M., Brunetti, M., Pergola, N., Serio, C., Vicente-Serrano, S. M., Tramutoli, V., & Ripullone, F. (2020). The impact of drought spells on

forests depends on site conditions: The case of 2017 summer heat wave in southern Europe. *Global Change Biology*, *26*(2), 851–863. https://doi.org/10.1111/gcb.14825

Ryan, M. G., & Law, B. E. (2005). Interpreting, measuring, and modeling soil respiration. *Biogeochemistry*, *73*(1), 3–27. https://doi.org/10.1007/s10533-004-5167-7

Sánchez-Benítez, A., García-Herrera, R., Barriopedro, D., Sousa, P. M., & Trigo, R. M. (2018). June 2017: The Earliest European Summer Mega-heatwave of Reanalysis Period. *Geophysical Research Letters*, *45*(4), 1955–1962. https://doi.org/10.1002/2018GL077253

Schimel, D., Stephens, B. B., & Fisher, J. B. (2015). Effect of increasing CO2 on the terrestrial carbon cycle. *Proceedings of the National Academy of Sciences*, *112*(2), 436–441. https://doi.org/10.1073/pnas.1407302112

Stocker, B. D., Zscheischler, J., Keenan, T. F., Prentice, I. C., Peñuelas, J., & Seneviratne, S. I. (2018). Quantifying soil moisture impacts on light use efficiency across biomes. *New Phytologist*, *218*(4), 1430–1449. https://doi.org/10.1111/nph.15123

Stocker, B. D., Zscheischler, J., Keenan, T. F., Prentice, I. C., Seneviratne, S. I., & Peñuelas, J. (2019). Drought impacts on terrestrial primary production underestimated by satellite monitoring. *Nature Geoscience*, *12*(4), 264–270. https://doi.org/10.1038/s41561-019-0318-6

Thornton, P. E., Lamarque, J.-F., Rosenbloom, N. A., & Mahowald, N. M. (2007). Influence of carbon-nitrogen cycle coupling on land model response to CO2 fertilization and climate variability. *Global Biogeochemical Cycles*, *21*(4). https://doi.org/10.1029/2006GB002868

Trucchia, A., Meschi, G., Fiorucci, P., Gollini, A., & Negro, D. (2022). Defining Wildfire Susceptibility Maps in Italy for Understanding Seasonal Wildfire Regimes at the National Level. *Fire*, *5*(1), 30. https://doi.org/10.3390/fire5010030

van der Woude, A. M., Peters, W., Joetzjer, E., Lafont, S., Koren, G., Ciais, P., Ramonet, M., Xu, Y., Bastos, A., Botía, S., Sitch, S., de Kok, R., Kneuer, T., Kubistin, D., Jacotot, A., Loubet, B., Herig-Coimbra, P.-H., Loustau, D., & Luijkx, I. T. (2023). Temperature extremes of 2022 reduced carbon uptake by forests in Europe. *Nature Communications*, *14*(1), 6218. https://doi.org/10.1038/s41467-023-41851-0

Vermote, E. (2015). MOD09A1 MODIS/Terra Surface Reflectance 8-Day L3 Global 500m SIN Grid V006 [Dataset]. NASA EOSDIS Land Processes Distributed Active Archive Center. https://doi.org/10.5067/MODIS/MOD09A1.006

Vicente-Serrano, S. M. (2007). Evaluating the Impact of Drought Using Remote Sensing in a Mediterranean, Semi-arid Region. *Natural Hazards*, *40*(1), 173–208. https://doi.org/10.1007/s11069-006-0009-7

Vicente-Serrano, S. M., Beguería, S., & López-Moreno, J. I. (2010). A Multiscalar Drought Index Sensitive to Global Warming: The Standardized Precipitation Evapotranspiration Index. *Journal of Climate*, *23*(7), 1696–1718. https://doi.org/10.1175/2009JCLI2909.1

Vicente-Serrano, S. M., Gouveia, C. M., Camarero, J. J., Beguería, S., Trigo, R., López-Moreno, J. I., Azorín-Molina, C., Pasho, E., Lorenzo-Lacruz, J., Revuelto, J., Morán-Tejeda, E., & Sanchez-Lorenzo, A. (2013). Response of vegetation to drought time-scales across global land biomes. *Proceedings of the National Academy of Sciences*, *110*(1), 52–57. https://doi.org/10.1073/pnas.1207068110

Vicente-Serrano, S. M., Lopez-Moreno, J.-I., Beguería, S., Lorenzo-Lacruz, J., Sanchez-Lorenzo, A., García-Ruiz, J. M., Azorin-Molina, C., Morán-Tejeda, E., Revuelto, J., Trigo, R., Coelho, F., & Espejo, F. (2014). Evidence of increasing drought severity caused by temperature rise in southern Europe. *Environmental Research Letters*, *9*(4), 044001. https://doi.org/10.1088/1748-9326/9/4/044001

von Buttlar, J., Zscheischler, J., Rammig, A., Sippel, S., Reichstein, M., Knohl, A., Jung, M., Menzer, O., Arain, M. A., Buchmann, N., Cescatti, A., Gianelle, D., Kiely, G., Law, B. E., Magliulo, V., Margolis, H., McCaughey, H., Merbold, L., Migliavacca, M., … Mahecha, M. D. (2018). Impacts of droughts and extreme-temperature events on gross primary production and ecosystem respiration: a systematic assessment across ecosystems and climate zones. *Biogeosciences*, *15*(5), 1293–1318. https://doi.org/10.5194/bg-15-1293-2018

Yang, H., Ciais, P., Frappart, F., Li, X., Brandt, M., Fensholt, R., Fan, L., Saatchi, S., Besnard, S., Deng, Z., Bowring, S., & Wigneron, J.-P. (2023). Global increase in biomass carbon stock dominated by growth of northern young forests over past decade. *Nature Geoscience*, *16*(10), 886–892. https://doi.org/10.1038/s41561-023-01274-4

Yu, P., Zhou, T., Luo, H., Liu, X., Shi, P., Zhang, Y., Zhang, J., Zhou, P., & Xu, Y. (2022). Global Pattern of Ecosystem Respiration Tendencies and Its Implications on Terrestrial Carbon Sink Potential. *Earth's Future*, *10*(8). https://doi.org/10.1029/2022EF002703

Zhang, Y., Xiao, X., Guanter, L., Zhou, S., Ciais, P., Joiner, J., Sitch, S., Wu, X., Nabel, J., Dong, J., Kato, E., Jain, A. K., Wiltshire, A., & Stocker, B. D. (2016). Precipitation and

carbon-water coupling jointly control the interannual variability of global land gross primary production. *Scientific Reports*, *6*(1), 39748. https://doi.org/10.1038/srep39748

Zhu, Z., Piao, S., Myneni, R. B., Huang, M., Zeng, Z., Canadell, J. G., Ciais, P., Sitch, S., Friedlingstein, P., Arneth, A., Cao, C., Cheng, L., Kato, E., Koven, C., Li, Y., Lian, X., Liu, Y., Liu, R., Mao, J., … Zeng, N. (2016). Greening of the Earth and its drivers. *Nature Climate Change*, *6*(8), 791–795. https://doi.org/10.1038/nclimate3004

Zscheischler, J., Mahecha, M. D., von Buttlar, J., Harmeling, S., Jung, M., Rammig, A., Randerson, J. T., Schölkopf, B., Seneviratne, S. I., Tomelleri, E., Zaehle, S., & Reichstein, M. (2014). A few extreme events dominate global interannual variability in gross primary production. *Environmental Research Letters*, *9*(3), 035001. https://doi.org/10.1088/1748-9326/9/3/035001

Zscheischler, J., Reichstein, M., von Buttlar, J., Mu, M., Randerson, J. T., & Mahecha, M. D. (2014). Carbon cycle extremes during the 21st century in CMIP5 models: Future evolution and attribution to climatic drivers. *Geophysical Research Letters*, *41*(24), 8853–8861. https://doi.org/10.1002/2014GL062409

References From the Supporting Information

Ballabio, C., Panagos, P., & Monatanarella, L. (2016). Mapping topsoil physical properties at European scale using the LUCAS database. *Geoderma*, *261*. https://doi.org/10.1016/j.geoderma.2015.07.006

ICOS RI. (2022). Ecosystem final quality (L2) product in ETC-Archive format - release 2022-1 (1.0) [Dataset]. ICOS ERIC - Carbon Portal. https://doi.org/10.18160/PAD9-HQHU

Kobayashi, K., & Salam, M. U. (2000). Comparing Simulated and Measured Values Using Mean Squared Deviation and its Components. *Agronomy Journal*, *92*(2), 345. https://doi.org/10.1007/s100870050043

Reichstein, M., Falge, E., Baldocchi, D., Papale, D., Aubinet, M., Berbigier, P., Bernhofer, C., Buchmann, N., Gilmanov, T., Granier, A., Grunwald, T., Havrankova, K., Ilvesniemi, H., Janous, D., Knohl, A., Laurila, T., Lohila, A., Loustau, D., Matteucci, G., … Valentini, R. (2005). On the separation of net ecosystem exchange into assimilation and ecosystem respiration: review and improved algorithm. *Global Change Biology*, *11*(9), 1424–1439. https://doi.org/10.1111/j.1365-2486.2005.001002.x

Saxton, K. E., & Rawls, W. J. (2006). Soil Water Characteristic Estimates by Texture and Organic Matter for Hydrologic Solutions. *Soil Science Society of America Journal*, *70*(5), 1569–1578. https://doi.org/10.2136/sssaj2005.0117

Villalba, G. (2024). Vegetation Photosynthesis and Respiration Model code and output for south-western Europe between 2001 and 2022 [Dataset]. Zenodo. https://doi.org/10.5281/ZENODO.10782550

Virtanen, P., Gommers, R., Oliphant, T. E., Haberland, M., Reddy, T., Cournapeau, D., Burovski, E., Peterson, P., Weckesser, W., Bright, J., van der Walt, S. J., Brett, M., Wilson, J., Millman, K. J., Mayorov, N., Nelson, A. R. J., Jones, E., Kern, R., Larson, E., … Vázquez-Baeza, Y. (2020). SciPy 1.0: fundamental algorithms for scientific computing in Python. *Nature Methods*, *17*(3), 261–272. https://doi.org/10.1038/s41592-019-0686-2

Warm Winter 2020 Team & ICOS Ecosystem Thematic Centre. (2022). Warm Winter 2020 ecosystem eddy covariance flux product for 73 stations in FLUXNET-Archive format—release 2022-1 (1.0) [Dataset]. ICOS Carbon Portal. https://doi.org/10.18160/2G60-ZHAK

Webber, H., Ewert, F., Olesen, J. E., Müller, C., Fronzek, S., Ruane, A. C., Bourgault, M., Martre, P., Ababaei, B., Bindi, M., Ferrise, R., Finger, R., Fodor, N., Gabaldón-Leal, C., Gaiser, T., Jabloun, M., Kersebaum, K.-C., Lizaso, J. I., Lorite, I. J., … Wallach, D. (2018). Diverging importance of drought stress for maize and winter wheat in Europe. *Nature Communications*, *9*(1), 4249. https://doi.org/10.1038/s41467-018-06525-2